J. Fluid Mech. (1987), *vol.* 180, *pp.* 267–295
Printed in Great Britain

Fast dynamo action in a steady flow

By A. M. SOWARD
School of Mathematics, The University, Newcastle upon Tyne, NE1 7RU, UK

(Received 24 January 1986 and in revised form 15 December 1986)

The existence of fast dynamos caused by steady motion of an electrically conducting fluid is established by consideration of a two-dimensional spatially periodic flow: the velocity, which is independent of the vertical coordinate z, is finite and continuous everywhere but the vorticity is infinite at the X-type stagnation points. A mean-field model is developed using boundary-layer methods valid in the limit of large magnetic Reynolds number R. The magnetic field is confined to sheets, width of order $R^{-\frac{1}{2}}$. The mean magnetic field lies and is uniform on horizontal planes; its direction is independent of time but rotates once about the vertical axis over a short distance $2\pi l$, where $l^{-1} = R^{\frac{1}{2}}\beta$ and β is a vertical stretched wavenumber independent of R. Its alternating direction gives it a rope-like structure within the sheets. An α-effect is calculated for the model, whose strength for a given flow is a function of β and R. Two sources of α-effect are isolated whose relative importance depends critically on the size of β. When the vorticity is finite everywhere and $\beta \ll 1$, the dynamo is 'almost' fast with growth rates of order $(\ln R)^{-1}$. The maximum growth rate $\ln(\ln R)/\ln R$ occurs when, correct to leading order, β is $(\ln R)^{-\frac{1}{2}}$. The asymptotic results valid for large R compare excellently with Roberts (1972) modal analysis for finite R.

1. Introduction

The kinematic dynamo problem is concerned with the magnetic field $\boldsymbol{b}(\boldsymbol{x}, t)$, induced by the motion of an electrically conducting fluid moving with velocity $\boldsymbol{u}(\boldsymbol{x}, t)$, in the absence of any external electric current sources. In dimensionless form $\boldsymbol{b}$ satisfies the magnetic induction equation

$$\boldsymbol{b}_{,t} = \nabla \times (\boldsymbol{u} \times \boldsymbol{b}) + R^{-1}\nabla^2 \boldsymbol{b}, \quad \nabla \cdot \boldsymbol{b} = 0, \tag{1.1a, b}$$

where R is the magnetic Reynolds number. For steady flows $\boldsymbol{u}(\boldsymbol{x})$, solutions of (1.1) can be sought in the form $\boldsymbol{b} = \mathrm{Re}\{\tilde{\boldsymbol{b}}(\boldsymbol{x})\, \mathrm{e}^{pt}\}$. When appropriate boundary conditions are applied as $|\boldsymbol{x}| \to \infty$, (1.1) reduces to an eigenvalue problem for the growth rate p. The dynamo is said to be 'fast' if $p \to p_0 (> 0)$ and slow if $p \downarrow 0$ as $R \uparrow \infty$. The existence of fast dynamos produced by steady motion is a controversial matter (e.g. see Zel'dovich, Ruzmaikin & Sokolov 1983; Moffatt & Proctor 1985; Soward & Childress 1986), which this paper partially resolves by consideration of an explicit dynamo model discussed previously by Childress (1979) in the large-R limit.

The existence of slow dynamos is well established and there are many known examples. One such example is Braginsky's (1964) nearly axially symmetric model of the geodynamo. Its main features are that the flow is dominated by large azimuthal velocities and that the field evolves on the slow magnetic diffusion timescale: i.e. $\boldsymbol{u}(\boldsymbol{x}, R^{-1}) \to \boldsymbol{u}(\boldsymbol{x}, 0)$ (azimuthal) and $p = O(R^{-1})$ as $R \uparrow \infty$. Though satisfactory as a description of the Earth's magnetic field, it is inappropriate for the Sun and other stars for which fields evolve on the faster convective timescale of the motion. In those

cases the possibility of fast dynamo action becomes an important question which is yet to be satisfactorily resolved.

For perfectly conducting fluids the solution of the magnetic induction equation is simple and given exactly by the Cauchy solution

$$b_i(\boldsymbol{X}, t) = b_j(\boldsymbol{x}, 0)\frac{\partial X_i}{\partial x_j}, \tag{1.2}$$

in which $\boldsymbol{X}$ is the position vector at time t of a fluid particle initially located at $\boldsymbol{x}$. Exponential growth of $\boldsymbol{b}$ is then guaranteed by the exponential growth of $\partial X_i/\partial x_j$. As Zel'dovich *et al.* (1983) point out this can be achieved by a simple linear straining motion. That is because the separation of two neighbouring particles increases indefinitely at an exponential rate. The flow is, however, unusual in that $|\boldsymbol{u}| \uparrow \infty$ as $|\boldsymbol{x}| \uparrow \infty$. Steady two-dimensional flows, like the velocity (2.1) below considered in this paper, are integrable and streamlines lie on surfaces. Consequently, $\partial X_i/\partial x_j$ can only grow exponentially at the stagnation points and elsewhere $\partial X_i/\partial x_j$ grows at most linearly. In three dimensions, steady flows can be non-integrable and in that context Dombre *et al.* (1986) have considered spatially periodic Beltrami flows for which $\boldsymbol{\omega} = \Lambda \boldsymbol{u}$, where $\boldsymbol{\omega}(= \nabla \times \boldsymbol{u})$ is the vorticity and Λ is a constant. Typical of the examples considered are ordered regions of spiralling vortices like the two-dimensional velocity (2.2) but intertwined between them are regions in which the particle paths are chaotic and $\partial X_i/\partial x_j$ grows exponentially. According to (1.2), therefore, exponential growth of the magnetic field may be possible.

The picture changes completely when the effects of small but finite diffusivity are considered. The reason is that, in the chaotic regions, the lengthscale of the magnetic field is reduced indefinitely and eventually diffusion necessarily becomes important. The structure of the magnetic field on the diffusive lengthscale is not determined by (1.2) and the exponential growth predicted by it is no longer applicable. Nevertheless, Arnol'd & Korkina (1983), Galloway & Frisch (1984, 1986) have investigated numerically solutions of (1.1) for particular three-dimensional spatially periodic Beltrami flows. Galloway & Frisch (1986) achieve high values of the magnetic Reynolds numbers and in that limit the magnetic field produced is concentrated into ropes inside the chaotic regions. They find no clear evidence of fast dynamo action. On the other hand, some of their results hint at the possibility and so they cautiously conclude that the matter remains unresolved.

Other recent investigations of fast dynamos have focused attention on the exponential growth of $\partial X_i/\partial x_j$ resulting from unsteady motion. Zel'dovich *et al.* (1983, 1984) considered a random motion, which at any instant is a linear straining motion, and demonstrated the exponential growth of the magnetic energy. Moffatt & Proctor (1985) have re-examined the stretch–twist–fold rope dynamo of Vainshtein & Zel'dovich (1972). The model, simple to conceive, is difficult to analyse with precision. The process pivots on a sequence of cycles, in which the magnetic flux of a rope is doubled: the fluid flow necessary to achieve the effect (cf. the doubling of an elastic band) is complicated. Nevertheless, Moffatt & Proctor (1985) provide some analytic quantification of the model. Without diffusion this fast dynamo leads to field structures on ever-decreasing lengthscales. The large but finite electrical conductivity means that eventually the field structure is controlled by diffusive processes. Indeed, Moffatt & Proctor (1985) make the stronger statement that, in general, the magnetic field produced by a fast dynamo must have a lengthscale of order $R^{-\frac{1}{2}}$ almost everywhere. This means, of course, that the field structure is singular in the limit $R \uparrow \infty$.

The idea, upon which the present paper is based, is that the stretch–twist–fold mechanism can be accomplished with magnetic-field topologies simpler than the closed loops of the Vainshtein & Zel'dovich (1972) rope dynamo. Consequently the corresponding motion necessary to achieve the effect is likely to be straightforward in comparison with that envisaged by Moffatt & Proctor (1985). In §2 a simple steady two-dimensional motion is described which leads to fast dynamo action: the magnetic field is certainly stretched, there is also twisting but no folding is necessary. The simplicity of the chosen motion highlights two significant points. They are that (i) exponential growth of $\partial X_i/\partial x_j$ is not a prerequisite for a fast dynamo; (ii) relative simplicity of the motion may be a desirable feature because it permits the magnetic field to arrange itself, and in particular its scale, necessarily on a length of order $R^{-\frac{1}{2}}$ (Moffatt & Proctor 1985), so that it can regenerate itself efficiently. Indeed, straining motion with chaotic $\partial X_i/\partial x_j$ may be very inefficient as much of the time fields with opposite orientations are likely to be brought into contact with each other leading to considerable mutual annihilation.

The paper is organized as follows. In §2 our two-dimensional motion is described and its relation to the earlier models of Roberts (1972) and Childress (1979) are explained. In §3 a heuristic picture of the mean-field dynamo is developed. The mathematical problem is reduced to determining the magnitude of an α-effect. That has two contributions which will be referred to as the 'stretch' and 'twist' mechanisms. The formal development of the mathematical model begins in §4. The governing equations are derived, the symmetry conditions are discussed, the ensuing boundary conditions are itemized and the resulting eigenvalue problem, for which the growth rate p is the eigenvalue, is formulated. The asymptotic analysis of the equations is restricted to the flux sheet boundary layers and the corner (or stagnation point) regions which connect them. They are considered in §§5 and 6 respectively. A comprehensive discussion of the solutions is given in §7. It bridges the formal and heuristic developments of the earlier sections and contains all the main quantitative results. Various limiting cases are discussed in §§7.1, 7.2 and 7.3, and from the results the maximum growth rate is determined in §7.4. The final §7.5 provides remarkable confirmation of the boundary-layer theory through excellent agreement with Roberts' (1972) numerical results based on a modal analysis at finite magnetic Reynolds number. A concluding remark is added in §8, and an analytic solution of the Childress (1979) problem (see §7.1) is derived in the Appendix.

2. The motion

Relative to rectangular Cartesian coordinates x, y, z Childress (1979) considered a class of two-dimensional spatially periodic flows for which the vertical z-velocity is constant on stream surfaces,

$$\boldsymbol{u} = \nabla\psi \times \hat{\boldsymbol{z}} + w(\psi)\,\hat{\boldsymbol{z}}, \tag{2.1}$$

where $\hat{\boldsymbol{z}}$ is the unit vector in the z-direction. For our purposes it is sufficient to study the family of spiralling vortices

$$w = K\psi, \quad \psi = a_\epsilon \sin x \sin y \tag{2.2a}$$

(see figure 1), where $K(>0)$ is a constant and $a_\epsilon = 1$ everywhere except within a small radius ϵ of every X-type stagnation point. It is defined to be

$$a_\epsilon(r) = 1 + \left[\ln\left(\frac{r}{\epsilon}\right)\right]^2 \quad (r < \epsilon \ll 1), \tag{2.2b}$$

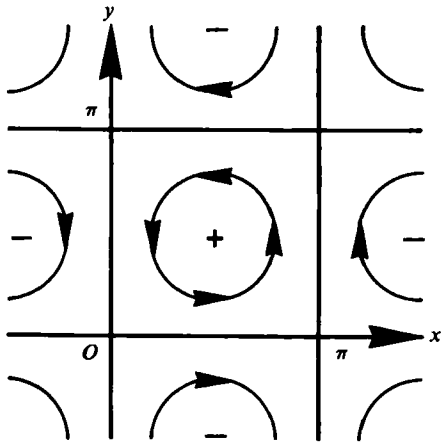

FIGURE 1. Projection of the streamlines in the (x, y)-plane with the sign of the z-component of velocity indicated.

where r is the radial distance from the stagnation point. (Near the origin: $r^2 = x^2+y^2$.) In the small regions $r < \epsilon$ the vertical vorticity ω has a weak singularity and is given to leading order by

$$\omega = -\frac{(8\ln(r/\epsilon)+2)xy}{r^2}. \tag{2.3}$$

On the other hand, the velocity itself remains finite and vanishes at the origin. Of course, the singularity of the vorticity at the stagnation point makes the flow difficult to achieve. Nevertheless, it could, in principle, be set up in a viscous fluid by body forces with integrable singularities at the stagnation points.

Guided by Childress' (1979) results it is anticipated that magnetic field is expelled from the cores of the vortices and confined to sheets where ψ is small, of order $R^{-\frac{1}{2}}$. These sheets expand in the corners where r is of order $R^{-\frac{1}{4}}$. An attractive feature of the motion (2.2) is that when

$$R^{-\frac{1}{4}} \ll \epsilon \ll 1 \tag{2.4}$$

the flow is almost uniform across the boundary layer $\psi = O(R^{-\frac{1}{2}})$. In fact, on the vortex boundary $0 < x < \pi$ the flow is given to leading order by

$$\psi_{,y}(x, 0) \equiv q_\epsilon(x) = a_\epsilon(x)\sin x, \tag{2.5a}$$

while in the corner region $r = O(R^{-\frac{1}{4}})$ it is defined to leading order by the stream function

$$\psi_\epsilon(x) = [\ln(R^{\frac{1}{4}}\epsilon)]^2 xy, \tag{2.5b}$$

and similarly near the corner $x = \pi, y = 0$. The latter, (2.5b), is, of course, the usual stagnation-point flow whose magnitude is bolstered up by the numerical factor $[\ln(R^{\frac{1}{4}}\epsilon)]^2$. The important feature of the modified flow is the acceleration into and out of the corner, which is achieved by the factor $a_\epsilon(x)$ in (2.5a). This has important repercussions for the results but has no influence on the boundary-layer calculations. For that reason our analysis of the Roberts' (1972), Childress' (1979), $\epsilon = 0$ flow applies equally well to the case $\epsilon \neq 0$.

An important characteristic of the flow is the vertical z-displacement 4δ of a fluid

particle after it has made a complete circuit of the stream surface, ψ = constant. In terms of the time taken 4τ it is

$$\delta = \tau w = K\psi\tau \quad (\delta = \delta(\psi), \quad \tau = \tau(\psi)). \tag{2.6}$$

On the vortex boundary $\psi = 0$ the velocity is given everywhere by (2.5a). The time taken from the stagnation point $(0, 0)$ to the edge $(\epsilon, 0)$ of the accelerated-flow region is $\frac{1}{2}\pi + O(\epsilon^2)$, of order unity, while the time taken to travel from $(\epsilon, 0)$ to $(\pi - \epsilon, 0)$ is $2\ln(\cot(\frac{1}{2}\epsilon))$, of order $\ln(\epsilon^{-1})$. The important point here is that the time taken to traverse the $R^{-\frac{1}{4}}$ corner region is never large, whatever the size of ϵ; it is the time taken to approach it that is long. The results stated indicate that

$$\tau \sim \begin{cases} -\ln\psi & (\epsilon^2 \ll \psi \ll 1), \quad (2.7a) \\ -2\ln\epsilon & (\psi \ll \epsilon^2). \quad (2.7b) \end{cases}$$

Here the $\psi \gg \epsilon^2$ streamsurfaces miss the accelerated-flow regions, while the $\psi \ll \epsilon^2$ streamsurfaces pass through them. To leading order the result implies that τ is constant in the boundary layer $\psi = O(R^{-\frac{1}{2}})$. In the limit $R \uparrow \infty$ with ϵ fixed it yields the result

$$\tau \sim \begin{cases} -2\ln\epsilon & (\epsilon \neq 0), \quad (2.8a) \\ \frac{1}{2}\ln R & (\epsilon = 0). \quad (2.8b) \end{cases}$$

From the dynamo point of view the important feature of the flow, (2.1), (2.2), is its helicity which, when $\epsilon = 0$, is

$$\boldsymbol{u}\cdot\boldsymbol{\omega} = K(\sin^2 x + \sin^2 y). \tag{2.9}$$

Since this pseudoscalar takes the same sign everywhere it follows that an α-effect can be identified which enables a mean-field dynamo to operate (see, for example, Moffatt 1978; Krause & Radler 1980). The fact that Beltrami flows have this property was pointed out originally by Childress (1967, 1970), who also noted the integrability of the two-dimensional case

$$K = \sqrt{2}, \quad \boldsymbol{\omega} = \sqrt{2}\boldsymbol{u}. \tag{2.10}$$

Roberts (1972), however, was the first to fully exploit the two-dimensional Beltrami motion (2.2) in the dynamo context and it is referred to in his paper as the 'first motion'.

A few brief remarks concerning the coordinate systems used are appropriate. For the boundary-layer calculations it is obviously convenient to have the Ox, Oy axes lying in the planes of the vortex boundaries. The modal analyses find it convenient to take axes Ox, Oy rotated by 45° about the vertical z-axis. Those are the axes adopted for the mean-field dynamo of Roberts (1972) and of Galloway & Frisch (1986), who also consider the two-dimensional motion. The rotation effects the length and velocity scales, and they must be carefully taken into account (see (7.38) below) when a comparison of the models is made.

3. A heuristic model

It is assumed that the mean magnetic field $\bar{\boldsymbol{b}}_{\mathrm{H}}(z, t)$ produced is independent of the horizontal x, y coordinates and so lies in horizontal planes. As already explained, all magnetic flux is expelled from the vortices and is confined to sheets on the vortex boundary where $\psi = O(R^{-\frac{1}{2}})$. The mean strength of these flux sheets is $\pi\bar{b}_x$ and $\pi\bar{b}_y$

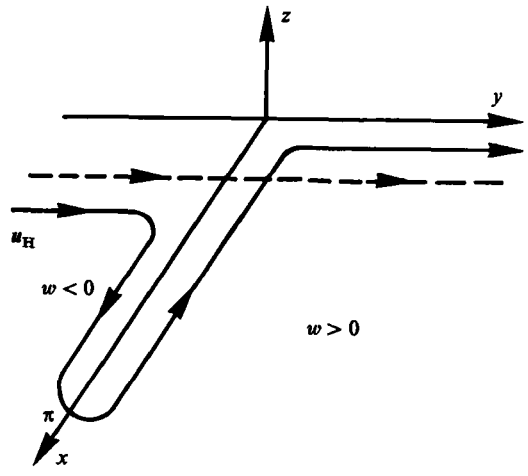

FIGURE 2. A typical field line (broken) parallel to the y-axis, together with its frozen displacement (solid) after application of the jerk. The horizontal u_H and vertical w motions are also indicated.

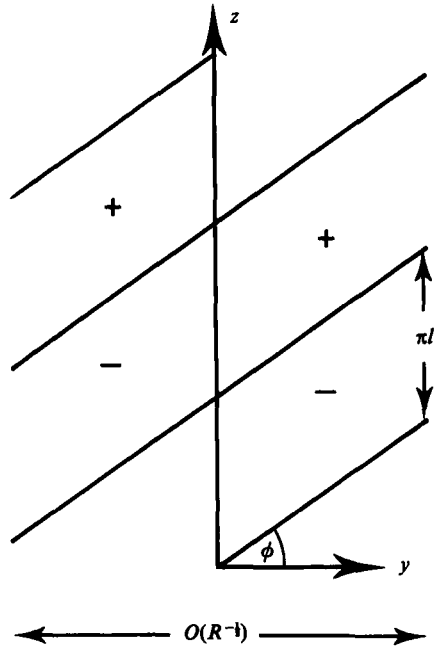

FIGURE 3. The sign of the x-component of magnetic field in the tilted tongues of figure 2, when the initial y-directed flux varies sinusoidally with z as in (3.1).

on the planes $y = n\pi$ and $x = m\pi$ respectively, where n and m are integers. Roberts (1972) has already provided a heuristic description of the finite-magnetic-Reynolds-number dynamo which is, of course, relevant to our model. Nevertheless, the picture presented here is more appropriate to the Childress (1979) boundary-layer development and is similar in spirit to the usual simplified description of the stretch–twist–fold rope dynamo.

Consider for the moment only the flux half-sheet $\frac{1}{2}\pi\bar{b}_y$ in the region $0 \leqslant x \leqslant O(R^{-\frac{1}{2}})$,

on the interval $-\pi < y < \pi$. Suppose that the motion is carried out in a jerk so that fluid particles in the boundary layer ($\psi = O(R^{-\frac{1}{2}})$) take up new positions instantaneously by application of the motion (2.2) for time τ (see (2.8)). The jerk produces a tongue of magnetic field, illustrated in figure 2, stretching along the x-axis from $x = 0$ to π. Simultaneously it is twisted by the vertical motion w which displaces and stretches it a vertical distance δ. The direct production of horizontal magnetic field in the tongues will be referred to as the 'stretch' mechanism. The production of vertical magnetic field by twisting with vertical stretching will be referred to as the 'twist' mechanism. They both contribute to the α-effect but their relative importance depends critically upon the vertical lengthscale l of the mean magnetic field produced (see (3.1) below).

The 'stretch' mechanism is simple to understand. Since the jerk doubles the length of field lines, their strength is also doubled. Nevertheless, the total flux $\frac{1}{2}\pi\bar{b}_y$ remains unaltered on the positive side of the y-axis, while exactly the same flux exists in the tongue but oppositely directed on either side of the x-axis. Specifically, fluxes of strength $\pm\frac{1}{2}\pi\bar{b}_y$ are located in the regions $0 \leqslant \mp y \leqslant O(R^{-\frac{1}{2}}), 0 < x < \pi$. Furthermore, if the original half-sheet $\frac{1}{2}\pi\bar{b}_y$ varies sinusoidally in the z-direction, say

$$\bar{b}_y = b(t)\sin\left(\frac{z}{l}\right) \quad (l = R^{-\frac{1}{2}}\beta^{-1}), \tag{3.1}$$

then the sign of the x-directed field in the tongues alternates on the length, πl. The vertical displacements $\delta(\psi)$ cause the layers to be tilted at an angle $\phi = O(\tan^{-1}(\mathrm{d}\delta/\mathrm{d}\psi))$, to the (x, y)-plane as illustrated in figure 3. In this way field of like sign is brought close together from either side of the plane $y = 0$ when

$$\frac{\mathrm{d}\delta}{\mathrm{d}\psi} \sim R^{\frac{1}{2}}l = \beta^{-1}. \tag{3.2}$$

To quantify the stretch effect, it simply assumed that all horizontal magnetic flux is displaced either up (when $\psi > 0$) or down (when $\psi < 0$) a constant distance

$$\delta_0 = -R^{-\frac{1}{2}}\alpha_S\,\tau, \tag{3.3a}$$

where, by (2.6),

$$\alpha_S = -K\xi_0, \quad \xi_0 = R^{\frac{1}{2}}\psi_0, \tag{3.3b}$$

and ξ_0, which is of order unity, measures the width of the flux sheet. Following the instantaneous displacement, the field is allowed to diffuse horizontally for time τ to smooth out its profile. Then the new flux $\pi\bar{b}_x(z, t+\tau)$, on the side $y = 0, 0 < x < \pi$, at height z is composed of the tongue fluxes described above and the x-directed fluxes resident on the sides before the jerk. With careful note of the original location of the fluxes, the new value is given by

$$2\bar{b}_x(z, t+\tau) = \bar{b}_y(z+\delta_0, t) - \bar{b}_y(z-\delta_0, t) + \bar{b}_x(z+\delta_0, t) + \bar{b}_x(z-\delta_0, t). \tag{3.4}$$

Provided $\bar{b}_H$ varies slowly on the time τ and on the length δ_0, specifically

$$l \gg \delta_0, \quad \text{or } R^{\frac{1}{2}}\beta\delta_0 \ll 1, \tag{3.5}$$

a Taylor series expansion of (3.4) yields

$$\bar{b}_{x,t} = -R^{-\frac{1}{2}}\alpha_S\bar{b}_{y,z} + R^{-1}\alpha_D\bar{b}_{x,zz} \quad (\alpha_D = \tfrac{1}{2}\alpha_S^2\tau). \tag{3.6}$$

The twist effect is less easy to understand and quantify because its influence on the magnetic field is spatially non-uniform. Evidently for a given vertical motion the strength of the vertical magnetic field KB produced in the tongue

$|y| \leqslant O(R^{\frac{1}{2}}), 0 < x < \pi$ is proportional to the time τ for which the flow acts, and the strength $\bar{b}_x$ of the original magnetic field from which it is produced. It follows that the total vertical magnetic flux in the tongue can be expressed in the form

$$K \int_{y_-}^{y_+} \int_0^{\pi} B \, \mathrm{d}x \, \mathrm{d}y = \pi R^{-\frac{1}{2}} \alpha_{\mathrm{T}} \tau \bar{b}_y \quad (R^{\frac{1}{2}} y_{\pm} = \pm \infty), \tag{3.7}$$

where α_{T} is a number dependent on R but not explicitly dependent on τ or $\bar{b}_y$. In addition (1.1b) gives

$$-R^{-\frac{1}{2}} \alpha_{\mathrm{T}} \tau \bar{b}_{y,z} = \bar{b}_x|_{x=\pi} - \bar{b}_x|_{x=0}, \tag{3.8a}$$

where now the bar is used to define the local average

$$\bar{b}_x = \pi^{-1} \int_{y_-}^{y_+} b_x \, \mathrm{d}y. \tag{3.8b}$$

Even when the non-uniformity of the flux $\pi \bar{b}_x$ is small, care must be taken to evaluate the flux difference in (3.8a) correctly. The simplest way to make a realistic estimate of its value is to measure the y-directed field at the origin (i.e. the point that is to be the tip of the tongue), and to measure the final x-directed field near the tip of the tongue at $x = \pi, y = 0$. The right-hand side of (3.8a) then measures the excess flux at $x = \pi$ over the value at $x = 0$ that it would have had if it were not for the twist effects under discussion. As a result, there is an additional term

$$-R^{-\frac{1}{2}} \alpha_{\mathrm{T}} \bar{b}_{y,z} \tag{3.9}$$

which must be added to the right-hand side of (3.6). It is difficult to make a sensible estimate of α_{T} on the basis of the jerk model. For, as the detailed analysis of §§4–6 below shows, its value is sensitive to the transverse diffusive mechanisms, which we have not attempted to quantify.

The effect of vertical diffusion of magnetic field can also be included in (3.6). With a similar equation for $\bar{b}_y$ the evolution of the complete horizontal mean magnetic field is governed by the dynamo equation

$$\bar{\boldsymbol{b}}_{\mathrm{H},t} = R^{-\frac{1}{2}} \nabla \times \alpha_{\mathrm{C}} \bar{\boldsymbol{b}}_{\mathrm{H}} + R^{-1}(1 + \alpha_{\mathrm{D}}) \bar{\boldsymbol{b}}_{\mathrm{H},zz}, \tag{3.10a}$$

where

$$\alpha_{\mathrm{C}} = \alpha_{\mathrm{S}} + \alpha_{\mathrm{T}} \tag{3.10b}$$

and α_{S} and α_{T} are of order unity. It admits solutions of the form

$$\bar{\boldsymbol{b}}_{\mathrm{H}} = b_0[\cos(R^{\frac{1}{2}} \beta z), \sin(R^{\frac{1}{2}} \beta z), 0)] \, \mathrm{e}^{pt} \tag{3.11a}$$

(see, for example, Moffatt 1970; Roberts 1972; Busse 1978) where b_0 is a constant and the growth rate p is given by

$$p = -\alpha_{\mathrm{C}} \beta - (1 + \alpha_{\mathrm{D}}) \beta^2. \tag{3.11b}$$

Of course, Roberts' (1972) heuristic picture of the dynamo also contained the ingredients of the stretch effect that we have attempted to quantify. The picture led him naturally to the solution (3.11), which for the steady flow (2.2) is valid for all values of β and R. The magnetic field it defines resembles a set of stacked ropes of horizontal width $O(R^{-\frac{1}{2}})$, and depth $O(R^{-\frac{1}{2}} \beta^{-1})$. In that sense it is a periodic version of the Vainshtein & Zel'dovich (1972) rope dynamo: the spatial periodicity obviates the need for the fold step in that model. The results of Roberts' (1972) numerical calculations are illustrated in figure 5 below. Childress' (1979) asymptotic results are valid in the limit of large R and small β (or more precisely $\beta \delta_0 \ll R^{-\frac{1}{2}} \ll 1$; see (3.5)).

In that case, the β^2 term in (3.11*b*) is negligible and the growth rate is $-\alpha_C\beta$. His boundary-layer analysis reveals that

$$\alpha_S = 2\alpha_C(<0), \quad \alpha_T = -\alpha_C(>0) \tag{3.12}$$

as we explain in §7.1 below.

The numerical value of α_C in the Childress limit (3.5) has caused some confusion. Childress' (1979) numerical procedures led to poor convergence but he, nevertheless, suggested that $2\alpha_C/K \doteqdot -1.03$. Anufriyev & Fishman (1982) repeated the calculation by a different method. They derived a number

$$Q = 0.37670\ldots, \tag{3.13a}$$

which they erroneously state leads to a value of α_C differing from that given above by about a factor 5. The confusion appears to have originated from two separate points; different scaling of ψ by the two authors, and a misprint in Childress (1979) of the value of $\int_0^\pi q_0\,\mathrm{d}x$, which was never subsequently used. When due account is taken of these points, the value of α_C is given by

$$\frac{2\alpha_C}{K} = -2\sqrt{2Q} = -1.06547\ldots. \tag{3.13b}$$

Our analytic solution (see (5.1*a*) and the Appendix, particularly (A 27)) confirms this value, which also agrees well with Roberts' (1972) results for finite R (see table 1 below).

To establish fast dynamo action it is sufficient that the growth rate (3.11*b*) has α_C given by the finite value (3.13*b*) for small fixed β in the limit $R\uparrow\infty$. This non-zero double limit cannot be achieved when $\epsilon = 0$. On the other hand, when $\epsilon \neq 0$, (2.8*a*) and (3.3*a*) imply that τ and $R^{\frac{1}{2}}\delta_0$ tend to constants as $R\uparrow\infty$. Consequently the inequality (3.5), necessary for the validity of the Childress (1979) theory, can be met when β is sufficiently small (but nevertheless fixed independent of R). These estimates are confirmed by the detailed analysis that follows in the later sections. There the theory is developed beyond the Childress limit and results are presented for

$$R^{\frac{1}{2}}\beta\delta_0 = O(1). \tag{3.14}$$

In addition the maximum growth rate is found (see (7.36) and (7.37)). The reader interested only in the results and not the mathematical details could omit §§4–6 and proceed directly to §7 where the solutions are discussed.

4. The mathematical model

Like Roberts (1972) it is assumed at the outset that the magnetic field may be expressed as the sum of modes of the type

$$\boldsymbol{b} = \mathrm{Re}\,[\boldsymbol{\mathcal{b}}(x_H)\exp(pt + \mathrm{i}R^{\frac{1}{2}}\beta z)], \tag{4.1a}$$

where here and elsewhere the subscript H is used to denote horizontal components, and

$$\boldsymbol{\mathcal{b}} = \boldsymbol{\mathcal{b}}_H + K\tilde{B}\hat{\boldsymbol{z}} \tag{4.1b}$$

is a complex vector in which the vertical magnetic field is scaled with the factor K. The horizontal components of the magnetic induction equation (1.1*a*) yield the equation

$$(\boldsymbol{u}_H\cdot\nabla + \lambda)\,\boldsymbol{\mathcal{b}}_H = \boldsymbol{\mathcal{b}}_H\cdot\nabla\boldsymbol{u}_H + R^{-1}\nabla_H^2\,\boldsymbol{\mathcal{b}}_H \tag{4.2a}$$

for $\boldsymbol{b}_H$, where

$$\lambda(\psi) = p + \beta^2 + iR_i^{\frac{1}{2}} K\beta\psi \tag{4.2b}$$

is complex and constant on streamsurfaces. According to (1.1b) the vertical magnetic field KB is given by

$$\nabla_H \cdot \boldsymbol{b}_H = -iR_i^{\frac{1}{2}} K\beta\tilde{B}. \tag{4.2c}$$

The vertical electric field E plays a central role in the theory. It is related to the vertical electric current J by Ohm's law

$$\hat{z}\cdot(\nabla_H \times \boldsymbol{b}_H) = \tilde{J} = R[\tilde{E} + \hat{z}\cdot(\boldsymbol{u}_H \times \boldsymbol{b}_H)]. \tag{4.3}$$

From (4.2a) it can be shown that $\tilde{E}$ satisfies

$$(\boldsymbol{u}_H \cdot \nabla_H + \lambda)\tilde{E} = R^{-1}(\lambda\tilde{J} + \nabla_H\lambda\cdot\nabla_H\tilde{B}), \tag{4.4a}$$

while from the vertical component of (1.1a) it can be shown, in addition, that $\tilde{B}$ satisfies

$$(\boldsymbol{u}_H \cdot \nabla_H + \lambda)\tilde{B} + \tilde{E} = R^{-1}(\tilde{J} + \nabla_H^2\tilde{B}). \tag{4.4b}$$

Guided by Roberts' (1972) analysis and results, solutions are sought, as in §3, for which the mean magnetic field is given by (3.11a) with p real. For convenience, the arbitrary constant b_0 is chosen to be π^{-1} so that

$$\langle \boldsymbol{b} \rangle = \pi^{-1}(1, -i, 0), \tag{4.5}$$

where the angled brackets are used to denote the horizontal average of tilded functions. The fluctuating part of the field, $\boldsymbol{b} - \langle \boldsymbol{b} \rangle$, has the same 2π-periodicity in the x- and y-directions as the flow, (2.2), and so attention may be restricted to the torus $[-\pi, \pi] \times [-\pi, \pi]$. Consistent with the governing equations, the reflectional symmetries in the planes $x = 0$, and $y = 0$ are accommodated by

$$\begin{bmatrix} \tilde{b}_x \\ \tilde{b}_y \\ \tilde{B} \end{bmatrix}(x, y) = \begin{bmatrix} \tilde{b}_x^* \\ -\tilde{b}_y^* \\ -\tilde{B}^* \end{bmatrix}(x, -y) = \begin{bmatrix} \tilde{b}_x^* \\ -\tilde{b}_y^* \\ \tilde{B}^* \end{bmatrix}(-x, -y) = \begin{bmatrix} \tilde{b}_x \\ \tilde{b}_y \\ -\tilde{B} \end{bmatrix}(-x, y), \tag{4.6}$$

where the star denotes complex conjugate. The assumed form (4.6) also takes into account the requirements of the mean field (4.5) in as much as $\tilde{b}_x$ and $i\tilde{b}_y$ are real on the x- and y-axes respectively. Again, consistent with the governing equations and the anticipated form (4.5) of the mean field, the rotational symmetries are met when

$$i\tilde{\boldsymbol{b}}(x, y) = [\hat{z} \times \boldsymbol{b}_H + K\tilde{B}\hat{z}](y, \pi - x). \tag{4.7}$$

The electric current $\tilde{J}$ and the electric field $\tilde{E}$ possess the same symmetries as $\tilde{B}$.

The symmetries mentioned were useful to Roberts (1972) because they enabled him to restrict attention to a subset of the Fourier coefficients in his modal expansions. For our asymptotic problem, on the other hand, it means that only one boundary layer, say the vortex boundary $0 < x < \pi, y = O(R^{-\frac{1}{2}})$, and X-type neutral point, say the origin $(x, y) = (0, 0)$, need be considered. They are discussed in detail in §§5 and 6.

The consistency of the assumed forms (3.11a), (4.5) for the mean magnetic field is finally established by averaging the magnetic induction equation (1.1a). It gives

$$(p + \beta^2)\langle \boldsymbol{b} \rangle = iR_i^{\frac{1}{2}}\beta\hat{z} \times \langle \boldsymbol{u} \times \boldsymbol{b} \rangle, \tag{4.8a}$$

and with the symmetry assumptions (4.6), (4.7) implies that

$$\langle \boldsymbol{u}\times\boldsymbol{b}\rangle = R^{-\frac{1}{3}}\alpha_{\mathrm{C}}\langle \boldsymbol{b}_{\mathrm{H}}\rangle - \mathrm{i}R^{-\frac{1}{3}}\beta\alpha_{\mathrm{D}}\,\hat{\boldsymbol{z}}\times\langle \boldsymbol{b}_{\mathrm{H}}\rangle, \tag{4.8b}$$

where the constants $\alpha_{\mathrm{C}}(\beta, R)$ and $\alpha_{\mathrm{D}}(\beta, R)$ satisfy

$$p+\beta^2 = -\alpha_{\mathrm{C}}\beta - \alpha_{\mathrm{D}}\beta^2 = -\alpha\beta \tag{4.8c}$$

(say). Since (4.7) implies that $\mathrm{i}\langle \boldsymbol{b}_{\mathrm{H}}\rangle$ equals $\hat{\boldsymbol{z}}\times\langle \boldsymbol{b}_{\mathrm{H}}\rangle$ it is impossible to distinguish the two terms in the centre of (4.8*c*). The constants α_{C} and α_{D} are, therefore, not unique and only the sum $\alpha\beta$ is meaningful. In the case of multiple-length-scale dynamos, such as the Childress (1979) limit (3.5), β is adopted as the expansion parameter and α is expressed by its Taylor series representation

$$\alpha(\beta) = \alpha(0) + \left(\frac{\mathrm{d}\alpha}{\mathrm{d}\beta}\right)(0)\,\beta + \ldots. \tag{4.8d}$$

Here $\alpha(0)$ is the α-effect and $(\mathrm{d}\alpha/\mathrm{d}\beta)(0)$ is the 'turbulent' diffusivity. For the parameter range (3.14) for which this paper is primarily concerned α is a complicated function of β, which we determine in the large-R limit (see figure 4*a* below).

In order to accomplish the generalizations cited to Childress' (1979) theory, the magnetic field $\boldsymbol{b}$ is expressed in the toroidal–poloidal form

$$\boldsymbol{b} = \boldsymbol{\nabla}\times A\hat{\boldsymbol{z}} + R^{-1}K\boldsymbol{\nabla}\times(\boldsymbol{\nabla}\times\phi\hat{\boldsymbol{z}}). \tag{4.9a}$$

The vertical magnetic field KB and electric current J are then given by

$$B = -R^{-1}\nabla_{\mathrm{H}}^2\phi, \quad J = -\nabla_{\mathrm{H}}^2 A, \tag{4.9b}$$

while the induction term in (4.3), which links E to J, is

$$\hat{\boldsymbol{z}}\cdot(\boldsymbol{u}_{\mathrm{H}}\times\boldsymbol{b}_{\mathrm{H}}) = -\boldsymbol{u}_{\mathrm{H}}\cdot\boldsymbol{\nabla}A + R^{-1}K\boldsymbol{\nabla}_{\mathrm{H}}\psi\cdot\boldsymbol{\nabla}_{\mathrm{H}}\phi_{,z}. \tag{4.10}$$

The z-component of the magnetic induction equation (1.1*a*) is

$$B_{,t} + \boldsymbol{u}_{\mathrm{H}}\cdot\boldsymbol{\nabla}_{\mathrm{H}}B = -\boldsymbol{u}_{\mathrm{H}}\cdot\boldsymbol{\nabla}_{\mathrm{H}}A + R^{-1}\boldsymbol{\nabla}_{\mathrm{H}}\cdot(w\boldsymbol{\nabla}_{\mathrm{H}}\phi_{,z}) + R^{-1}\nabla^2 B. \tag{4.11}$$

The inverse curl of (1.1*a*) introduces the gradient of a potential $R^{-\frac{1}{3}}K\chi$. The z-component of that equation is

$$A_{,t} = R^{-\frac{1}{3}}K\chi_{,z} - E + R^{-1}A_{,zz}, \tag{4.12}$$

while the remaining horizontal components yield

$$\boldsymbol{\nabla}_{\mathrm{H}}\chi = R^{\frac{1}{3}}(B\boldsymbol{\nabla}_{\mathrm{H}}\psi - \psi\boldsymbol{\nabla}_{\mathrm{H}}A) + \boldsymbol{P}_{\mathrm{H}}\times\hat{\boldsymbol{z}}, \tag{4.13a}$$

where

$$\boldsymbol{P}_{\mathrm{H}} = R^{-\frac{1}{3}}[\boldsymbol{\nabla}_{\mathrm{H}}\phi_{,t} + K\psi\boldsymbol{\nabla}_{\mathrm{H}}\phi_{,z} - R^{-1}\nabla^2(\boldsymbol{\nabla}_{\mathrm{H}}\phi)]. \tag{4.13b}$$

In terms of the complex tilded variables, (4.12) becomes

$$\tilde{E} = \beta(\alpha\tilde{A} + \mathrm{i}K\tilde{\chi}), \tag{4.14}$$

where α is defined by (4.8*c*), while (4.11) is closely linked with (4.4*b*). The component of (4.13*a*) normal to the streamsurfaces, namely

$$\boldsymbol{\nabla}_{\mathrm{H}}\psi\cdot\boldsymbol{\nabla}_{\mathrm{H}}\tilde{\chi} = R^{\frac{1}{3}}(|\boldsymbol{\nabla}_{\mathrm{H}}\psi|^2\tilde{B} - \psi\boldsymbol{\nabla}_{\mathrm{H}}\psi\cdot\boldsymbol{\nabla}_{\mathrm{H}}\tilde{A}) - R^{-\frac{1}{3}}\lambda\boldsymbol{u}_{\mathrm{H}}\cdot\boldsymbol{\nabla}_{\mathrm{H}}\tilde{\phi} - R^{-\frac{1}{3}}\boldsymbol{u}_{\mathrm{H}}\cdot\boldsymbol{\nabla}_{\mathrm{H}}\tilde{B}, \tag{4.15}$$

is particularly important because it can be used to determine $\tilde{\chi}$ in (4.14) (see (5.9) below).

Since magnetic field is confined to streamsurfaces $\psi = O(R^{-\frac{1}{2}})$ the stretched stream function $\xi = R^{\frac{1}{2}}\psi$ is introduced (see (5.2b) below) and it is assumed that

$$\boldsymbol{b}_{\mathrm{H}} \to 0, \quad \tilde{B} \to 0, \quad \tilde{J} \to 0, \quad \tilde{E} \to 0 \quad \text{as } \xi \to \infty. \tag{4.16a}$$

Inside the square $0 \leqslant x \leqslant \pi, 0 \leqslant y \leqslant \pi$ but outside the boundary layer it is convenient to assume, in addition, that

$$\tilde{A} \to 0, \quad \tilde{\phi} \to 0 \quad \text{as } \xi \to \infty. \tag{4.16b}$$

With attention restricted to the boundary layer $0 < x < \pi, \xi = O(1)$. Only the half-layer $\xi \geqslant 0$ need be considered provided symmetry conditions on $y = 0$ are met. According to (4.6) they are

$$\begin{bmatrix} b_{x\mathrm{r},y} & b_{y\mathrm{r}} & B_{\mathrm{r}} & J_{\mathrm{r}} & E_{\mathrm{r}} \\ b_{x\mathrm{i}} & b_{y\mathrm{i},y} & B_{\mathrm{i},y} & J_{\mathrm{i},y} & E_{\mathrm{i},y} \end{bmatrix} = [0], \tag{4.17}$$

where the extra subscripts r and i denote the real and imaginary parts respectively. Note, however, that the symmetry arguments leading to (4.17) do not extend to the potentials $\tilde{A}$, $\tilde{\phi}$ and $\tilde{\chi}$ because of the choice of boundary conditions (4.16b).

5. The boundary layer

The boundary-layer analysis proceeds on the basis that the parameters

$$\nu = -\frac{\alpha}{K}, \quad \mu = K\beta\tau, \tag{5.1a}$$

are both of order unity and that, in particular,

$$\nu = O(1), \quad \mu = O(1), \quad R \gg \tau \gg 1 \tag{5.1b}$$

(see (3.3), (3.14)). Consistent with these assumptions it is assumed that

$$\lambda = O(K\beta), \quad \tilde{A} = O(1), \quad \tilde{B} = O(1), \quad \tilde{E} = O(K\beta). \tag{5.1c}$$

In the boundary layer, $0 < x < \pi, \psi = O(R^{-\frac{1}{2}})$, excluding the corner regions, we follow Childress (1979) and adopt the boundary-layer coordinates

$$\sigma = \int_0^x q \, \mathrm{d}x, \quad \xi = R^{\frac{1}{2}}\psi, \tag{5.2a, b}$$

where the flow velocity $q(\equiv q_0)$ can be expressed in the form

$$q = [\sigma(2-\sigma)]^{\frac{1}{2}} \tag{5.2c}$$

(see (2.5a)). The coordinate σ varies from 0 at $x = 0$ to 2 at $x = \pi$. The boundary-layer approximations, which follow, are valid provided that

$$K\beta \ll \sigma \text{ (and } 2-\sigma). \tag{5.3}$$

The y-component of magnetic field on the boundary $y = 0$ is obtained from (4.10) upon division by q. In terms of the boundary-layer coordinates it is, correct to leading order,

$$-\tilde{A}_{,x} + \mathrm{i}K\beta R^{-\frac{1}{2}}\tilde{\phi}_{,y} = -q\tilde{A}_{,\sigma} - \mathrm{i}K\beta q^{-1}\bar{C} \quad (\xi = 0, \quad 0 < \sigma < 2), \tag{5.4a}$$

where

$$\bar{C} = -\int_\xi^\infty \tilde{B} \, \mathrm{d}\xi. \tag{5.4b}$$

The symmetry condition $\tilde{b}_{yr}(x,0)=0$ (see (4.17)) then yields

$$\tilde{A}_{r,\sigma}=K\beta q^{-2}\tilde{C}_1 \quad (\xi=0, \quad 0<\sigma<2). \tag{5.5}$$

In view of our basic assumptions (5.1) and (5.3), the right-hand side of (5.5) is ignored and the normalization condition (4.5) implies

$$\tilde{A}_r=-1 \quad (\xi=0, \quad 0<\sigma<2). \tag{5.6}$$

On the other hand, the x-component of magnetic field on the boundary $y=0$ is given correct to leading order simply by

$$\tilde{A}_{,y}=R^{\frac{1}{2}}q\tilde{A}_{,\xi} \quad (\xi=0, \quad 0<\sigma<2), \tag{5.7}$$

where the term neglected is of order $R^{-\frac{1}{2}}K\beta$. It follows that the symmetry condition, $\tilde{b}_{x1}(x,0)=0$ (see (4.17)) is met when

$$\tilde{A}_{1,\xi}=0 \quad (\xi=0, \quad 0<\sigma<2). \tag{5.8}$$

The cumbersome equation (4.15) provides the key to the evaluation of the α-effect. At leading order it simplifies considerably,

$$\tilde{\chi}_{,\xi}=\tilde{B}-\xi\tilde{A}_{,\xi}, \tag{5.9a}$$

and integrates to give

$$\tilde{\chi}=\tilde{C}+\int_{\xi}^{\infty}\xi' A_{,\xi'}\,\mathrm{d}\xi'. \tag{5.9b}$$

It follows immediately from (4.14) and the symmetry condition $E_r(x,0)=0$ on the electric field that

$$\alpha=\alpha_S+\alpha_T, \tag{5.10a}$$

where

$$\left.\begin{aligned}\alpha_S&=-K\int_0^{\infty}\xi\tilde{A}_{1,\xi}\,\mathrm{d}\xi\\ \alpha_T&=K\int_0^{\infty}\tilde{B}_1\,\mathrm{d}\xi\end{aligned}\right\}\ (0<\sigma<2) \tag{5.10b}$$

(cf. (3.3b) and (3.7) respectively). Though α is a constant, the parameters α_S and α_T are, in general, functions of σ. Nevertheless, within the framework of the governing equations (5.11), and the approximate boundary conditions (5.8), (5.12), both α_S and α_T are constants correct to leading order.

The diffusion equations governing $\tilde{A}$ and $\tilde{B}$ may be deduced from (4.12) and (4.11). To leading order they are the same as those given by Childress (1979), namely

$$\tilde{A}_{,\sigma}=\tilde{A}_{,\xi\xi}, \tag{5.11a}$$

$$\tilde{B}_{,\sigma}=\tilde{B}_{,\xi\xi}-\tilde{A}_{,\sigma}. \tag{5.11b}$$

Together with (5.9a) they yield the single equation

$$\tilde{F}_{,\sigma}=\tilde{F}_{,\xi\xi}, \tag{5.11c}$$

which replaces (5.11b) and where

$$\tilde{F}=\tilde{C}+\tilde{\chi}. \tag{5.11d}$$

In view of the symmetry of $\tilde{B}$ and the approximations (5.6), (5.8) to the boundary conditions on $\tilde{A}$, the corresponding boundary conditions applicable to $\tilde{F}$ are, correct to leading order,

$$\tilde{F}_{r,\xi}=0, \quad \tilde{F}_1=\tilde{F}_1^{(1)}(0) \quad (\xi=0, \quad 0<\sigma<2), \tag{5.12}$$

where, in the notation of §6, $\tilde{F}_1^{(1)}(0)$ is a constant independent of σ. The solutions of (5.11a, c), which satisfy the boundary conditions (5.6), (5.8) and (5.12), are

$$\tilde{A}(\sigma,\xi) = -\operatorname{erfc}\left[\frac{\xi}{(4\sigma)^{\frac{1}{2}}}\right]+\frac{1}{2}\int_0^\infty [G(\sigma,\xi-\xi')\,\tilde{A}(0,\xi')-G(\sigma,\xi+\xi')\,\tilde{A}^*(0,\xi')]\,\mathrm{d}x', \tag{5.13a}$$

$$\tilde{F}(\sigma,\xi) = \mathrm{i}\tilde{F}_1^{(1)}(0)\operatorname{erfc}\left[\frac{\xi}{(4\sigma)^{\frac{1}{2}}}\right]+\frac{1}{2}\int_0^\infty [G(\sigma,\xi-\xi')\,\tilde{F}(0,\xi')+G(\sigma,\xi+\xi')\,\tilde{F}^*(0,\xi')]\,\mathrm{d}\xi', \tag{5.13b}$$

where G is the Green function

$$G(\sigma,\xi) = (\pi\sigma)^{-\frac{1}{2}}\,\mathrm{e}^{-\xi^2/4\sigma}. \tag{5.13c}$$

The solution (5.13) is used to link the outflow values of the electromagnetic field at the corner $\sigma = 0$ to the inflow values at the corner $\sigma = 2$.

6. The corner region

In this section the corner region, near the origin (say), is defined by

$$\sigma \ll 1. \tag{6.1}$$

This means that the corner and boundary layer have the overlap region

$$K\beta \ll \sigma \ll 1, \tag{6.2}$$

in which formal matching of solutions can be achieved. Similar results apply to the corner at $x = \pi, y = 0$. As Childress (1979) has explained, horizontal diffusion, which is important in fixing the boundary-layer structure (see (5.11)), becomes negligible as the stagnation point $x = \pi, y = 0$ is approached. In the corner regions (4.4a, b) are appropriate with the horizontal diffusion terms on their right-hand sides ignored. They are readily solved and yield the results

$$\tilde{E}^{(\mathrm{o})} = \mathrm{e}^{-\lambda\tau}\tilde{E}^{(\mathrm{i})}, \tag{6.3a}$$

$$\tilde{B}^{(\mathrm{o})} = \mathrm{e}^{-\lambda\tau}(\tilde{B}^{(\mathrm{i})}-\tau\tilde{E}^{(\mathrm{i})}), \tag{6.3b}$$

where the superscripts i and o distinguish the inflow and outflow values respectively, and from (4.2b), (4.8c) λ is

$$\lambda = -\alpha\beta+\mathrm{i}K\beta\xi. \tag{6.3c}$$

The time τ taken to pass the corner is, like λ, a function of ξ (see (2.7)). Nevertheless to leading order τ is a constant (see (2.8)).

To complete the boundary-layer problem, it is necessary to link the inflow and outflow values of $\tilde{A}$ and $\tilde{F}$, as indicated in §5 above. First, it is easy to show from (6.3a, b) that

$$\tilde{E}^{(\mathrm{o})}_{,\xi}-\mathrm{i}K\beta\tilde{B}^{(\mathrm{o})} = \mathrm{e}^{-\lambda\tau}\{\tilde{E}^{(\mathrm{i})}_{,\xi}-\mathrm{i}K\beta\tilde{B}^{(\mathrm{i})}\} \tag{6.4}$$

and together with (4.14) and (5.9a) they yield the result

$$A^{(\mathrm{o})}_{,\xi} = \mathrm{e}^{-\lambda\tau}A^{(\mathrm{i})}_{,\xi}, \tag{6.5a}$$

where, by (5.1a) and (6.3c),

$$\lambda\tau = \mu(\nu+\mathrm{i}\xi). \tag{6.5b}$$

Secondly, it follows from (4.14), (5.9b) and (5.11d) that

$$K\tilde{F} = -2\mathrm{i}\beta^{-1}\tilde{E}-\int_\xi^\infty (2\mathrm{i}\alpha+K\xi')\,\tilde{A}_{,\xi'}\,\mathrm{d}\xi'. \tag{6.6}$$

Together with (6.3*a*) and (6.5) it gives

$$\tilde{F}^{(0)} = \tilde{F}^{(1)}\,\mathrm{e}^{-\lambda\tau} + \mathrm{e}^{-\mu\nu}\int_{\xi}^{\infty} (2\mathrm{i}\nu - \xi')\,(\mathrm{e}^{-\mathrm{i}\mu\xi'} - \mathrm{e}^{-\mathrm{i}\mu\xi})\,A^{(1)}_{,\xi}\,\mathrm{d}\xi'. \tag{6.7}$$

The link between the $\sigma = 0$ and $\sigma = 2$ solutions (see (5.13)) is completed by noting that the symmetries (4.7) imply

$$\tilde{A}_{,\xi}(0,\xi) = \mathrm{i}\tilde{A}^{(0)}_{,\xi}(\xi), \quad \tilde{F}(0,\xi) = \mathrm{i}\tilde{F}^{(0)}(\xi), \tag{6.8a}$$

where

$$\tilde{A}_{,\xi}(2,\xi) = \tilde{A}^{(1)}_{,\xi}(\xi), \quad \tilde{F}(2,\xi) = F^{(1)}(\xi). \tag{6.8b}$$

The only remaining detail over which some care must be taken is whether the outflow values achieved as $\xi \downarrow 0$ are equal to the applied values on $\xi = 0$. For example, it is clear from the nature of the heat-conduction solution for $\tilde{A}$ that

$$\lim_{\xi\downarrow 0} \tilde{A}^{(0)}_{\mathrm{i}} \neq -\tilde{A}_{\mathrm{r}}(0,0) = 1, \tag{6.9}$$

in contradiction with the outflow boundary condition (5.6). This means that a further boundary layer is triggered at the corners, as recognized by Childress (1979) and analysed subsequently by Anufriyev & Fishman (1982). Here the flow velocity is slow, magnetic induction is negligible and the electric current is given by Ohm's law

$$\tilde{E} = R^{-1}\tilde{J} \tag{6.10}$$

for a stationary conductor. This provides the dominant balance in both (4.4*a* and *b*). Furthermore (5.9) remains valid and, since $\tilde{B}$ and $\xi\tilde{A}_{,\xi}$ stay finite, $\tilde{\chi}$ suffers no jump in value. It follows from (4.14), (6.9) that $\tilde{E}_{\mathrm{i}}$ is discontinuous,

$$\lim_{\xi\downarrow 0} \tilde{E}^{(0)}_{\mathrm{i}} = \alpha\beta\,(\lim_{\xi\downarrow 0} \tilde{A}^{(0)}_{\mathrm{i}} - 1) \neq -\tilde{E}_{\mathrm{r}}(0,0) = 0. \tag{6.11}$$

The fact that both $\tilde{\chi}$ and $\tilde{C}$ are continuous on the outflow boundary is important because continuity of $\tilde{F}$ is then implied by (5.11*d*). With (6.8*b*) it yields the result

$$\tilde{F}^{(1)}_{\mathrm{i}}(0) = \lim_{\xi\downarrow 0} F^{(0)}_{\mathrm{r}}, \tag{6.12}$$

which provides the one remaining boundary condition necessary to complete the mathematical formulation of the boundary-layer problem.

In the discussion of the solutions, which follows, μ and ν (see (5.1*a*)) provide convenient measures of β and α respectively. In terms of our principal boundary-layer functions, $\tilde{A}$ and $\tilde{F}$, the expressions (5.10) for α become

$$\nu = \nu_{\mathrm{S}} + \nu_{\mathrm{T}}, \tag{6.13a}$$

where use of (5.9*b*), (5.11*d*) yields

$$\nu_{\mathrm{S}} = \int_0^{\infty} \xi\tilde{A}^{(1)}_{\mathrm{i},\xi}\,\mathrm{d}\xi, \tag{6.13b}$$

$$2\nu_{\mathrm{T}} = \tilde{F}^{(1)}_{\mathrm{i}}(0) - \nu_{\mathrm{S}}. \tag{6.13c}$$

7. The solutions

Before discussing the nature of the solutions, some additional clarification of the stretch and twist dynamo mechanisms is appropriate, which relates the formal analysis of the previous sections with the heuristic development of §3. To that end

the boundary-layer equations for the flux sheet $0 < x < \pi, y = O(R^{-\frac{1}{2}})$ are averaged locally as defined by (3.8b). Equation (1.1b) (or (4.2c)) gives

$$\bar{b}_{x,x} = -K\bar{B}_{,z}, \tag{7.1a}$$

while the x-component of the magnetic induction equation (1.1a) (or (4.2a)) yields

$$\bar{b}_{x,t} + q\bar{b}_{x,x} - R^{-1}\bar{b}_{x,zz} = -(\overline{wb}_x)_{,z}. \tag{7.1b}$$

The left-hand side of (7.1b) describes the convection and diffusion of a passive scalar. The source term on the right is, in the notation of §4,

$$-(\overline{wb}_x)_{,z} \sim -\pi^{-1}R^{-\frac{1}{2}}K\left[\int_{-\infty}^{\infty} \xi A_{,\xi}\,\mathrm{d}\xi\right]_{,z}. \tag{7.2}$$

Here the vertical transport of magnetic flux $\pi\overline{wb}_x$ forms the basis of the heuristic picture of the α-'stretch' effect (see (3.4), (3.6)). Likewise, the advection term on the left of (7.1b), namely

$$-q\bar{b}_{x,x} = K(\overline{qB})_{,z} \sim \pi^{-1}R^{-\frac{1}{2}}K\left[\int_{-\infty}^{\infty} B\,\mathrm{d}\xi\right]_{,z}, \tag{7.3}$$

provides, in the heuristic picture, the basis of the α-'twist' effect (see (3.7), (3.8a)). The formal identification of (7.2) and (7.3) with α_S and α_T is given by (5.10).

The mathematical problem formulated in (5.13), (6.3c), (6.5), (6.7), (6.8), (6.12) and (6.13) was solved numerically. Equations for the inflow values of the four functions $A_{r,\xi}^{(i)}, A_{i,\xi}^{(i)}, F_r^{(i)}, F_i^{(i)}$ at $N+1$ equally spaced points, $\xi_n = n\xi_1 (0 \leqslant n \leqslant N)$, were set up and solved by a Newton–Raphson method. The value of N and the separation of points ξ_1 necessary for satisfactory convergence varied with μ. The magnitude of the eigenvalue ν (the magnitude of the α-effect, see (5.1a)) is plotted versus μ (a measure of β, see (5.1a)) in figure 4(a). The relative importance of the 'stretch' and 'twist' effects are made clear in figure 4(b), where, in addition to ν, the magnitude of ν_S is also plotted versus μ. The computed function $\nu(\mu)$ gives the growth rate

$$p = \tau^{-1}\mu\nu - (K\tau)^{-2}\mu^2 \tag{7.4}$$

(see (4.8c)), which highlights several interesting limits discussed in detail in the following subsections. Before proceeding, we note that K appears for the first time, as an independent parameter, in the vertical diffusion term of (7.4). Elsewhere K and β have always appeared as the product $K\beta$.

7.1. *The case* $\mu \ll 1$

In the Childress (1979) limit

$$\mu \ll 1 \tag{7.5}$$

the problem has an analytic solution which is derived for the first time in the Appendix. It gives

$$\nu = \nu_C + O(\mu), \tag{7.6}$$

where the number ν_C is defined by (A 27). This result provides a useful check on the numerical scheme. In particular, ν_C is given correct to four significant figures when $N = 48$, $\xi_1 = 0.5$ and $\xi_N = 24.0$.

When μ is a small fixed positive number, it follows from (2.8), (7.4) and (7.6) that, correct to leading order, positive growth rates,

$$p \sim \begin{cases} \frac{1}{2}\mu\nu_C/\ln(\epsilon^{-1}) & (\epsilon \neq 0), \qquad (7.7a) \\ 2\mu\nu_C/\ln R & (\epsilon = 0), \qquad (7.7b) \end{cases}$$

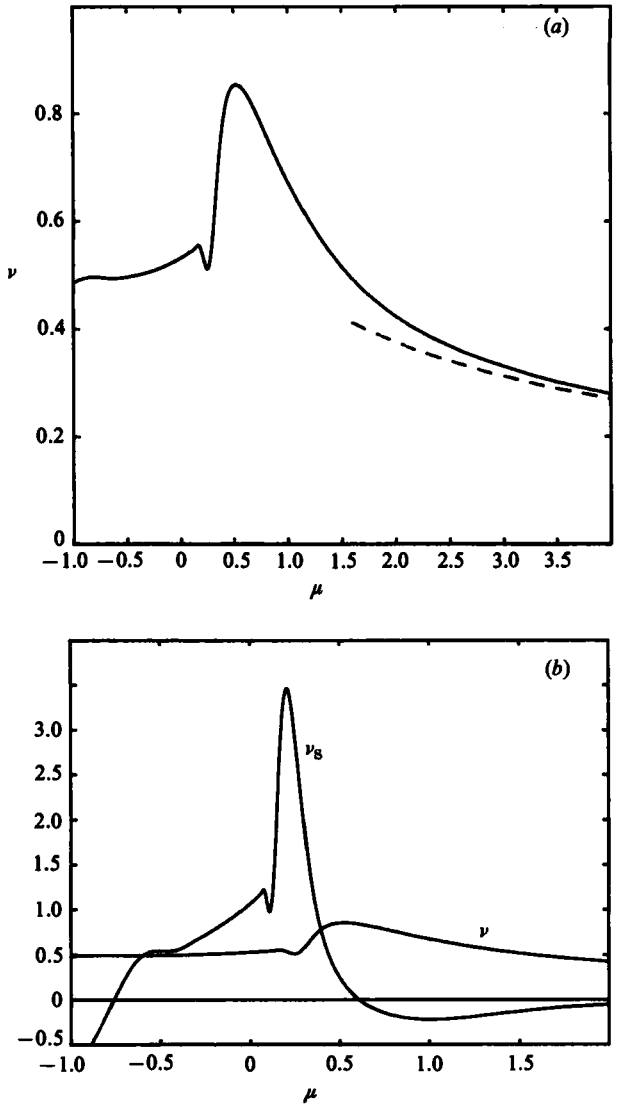

FIGURE 4. (*a*) The eigenvalue ν (the α-effect) plotted versus μ (the wavenumber). The results of the complete numerical problem are given by the solid line, while the asymptotic result (7.33) is denoted by the broken line. (*b*) The eigenvalue ν and ν_S (the α-'stretch' effect) plotted versus μ. Note that the scale is different to figure 4 (*a*), and that ν_T (the α-'twist' effect) is $\nu - \nu_S$ (not plotted).

are achieved in the limit $R \uparrow \infty$. It follows from (7.7*a*) that the weakly singular $\epsilon \neq 0$ flow is a fast dynamo. On the other hand, the Roberts (1972), Childress (1979) $\epsilon = 0$ flow is not a fast dynamo in the usual sense. Nevertheless, it is very efficient and predicts growth rates larger than any inverse power of R (i.e. (7.7*b*) implies $p \gg O(R^{-n})$ for all positive n). We, therefore, call it an 'almost' fast dynamo.

The small-μ assumption leads to a number of simplifications in the boundary-layer problem. The most important stems from the fact that $\lambda\tau$ is of order μ. It implies that the factor $e^{-\lambda\tau}$ in (6.5) takes the value unity and so leads to the result

$$\bar{A}(0,\xi) = i\bar{A}(2,\xi) \quad (\xi > 0), \tag{7.8}$$

central to the analysis of the Appendix. Since μ is absent from (7.8), the problem for $\bar{A}(\sigma, \xi)$ can be solved independent of $\bar{F}$. With $\bar{A}$ known and of order unity, it follows from (5.13b) and (6.7) that

$$\bar{F} = O(\mu). \tag{7.9}$$

According to (6.13), this result implies that $\bar{F}$ does not make a significant contribution to the value of the α-effect. Indeed, the stretch and twist contributions α_S and α_T given by (3.12) are based on the result $\nu_C = \frac{1}{2}\nu_S = -\nu_T$ derived from (6.13).

The essential feature of the Childress (1979) model described is the lengthscale l in the z-direction (see (3.1) above) which is long compared to the short horizontal length of order $R^{-\frac{1}{2}}$. It means that z-dependence may be ignored† in the α-effect calculation and so the vector potential A satisfies the two-dimensional heat conduction equation

$$(\boldsymbol{u}_H \cdot \nabla) A = R^{-1} \nabla_H^2 A \tag{7.10}$$

(see (4.3), (4.9b), (4.10) and (4.12)). Since horizontal diffusion is negligible in the corner regions (see §6), A enters and leaves with the same values (see (7.8)). Childress (1979) considered the effect of the $\boldsymbol{u}_H$ motion on a mean magnetic field uniform in the x-direction. It leads to the well-known problem of flux expulsion for which the first numerical simulations were performed by Weiss (1966); our analytic solution appears in the Appendix. Childress (1979) determines the vertical field KB, just as here, on the basis that $F = 0$ (see (7.9)) with the consequence that

$$B = \tfrac{1}{2}\xi A_{,\xi}. \tag{7.11}$$

His α-effect calculation is reduced to the evaluation of the boundary-layer integrals which appear in (7.2) and (7.3), giving

$$\alpha(0) = -K\nu_C \tag{7.12}$$

in (4.8d).

Unlike the α-effect $\alpha(0)$, which is fixed at leading order, the 'turbulent' diffusivity

$$\left(\frac{\mathrm{d}\alpha}{\mathrm{d}\beta}\right)(0) = -K^2\tau\left(\frac{\mathrm{d}\nu}{\mathrm{d}\mu}\right)(0) \tag{7.13a}$$

(see (4.8d)), is determined by the order-μ terms in our expansions. It is comparable with the molecular diffusivity when

$$K^{-2} = O(\tau). \tag{7.13b}$$

The numerical results illustrated in figure 4 (a) show clearly that $(\mathrm{d}\nu/\mathrm{d}\mu)(0)$ is positive implying a negative value for the diffusivity (7.13a). This result contrasts dramatically with the heuristic arguments of §3 which led to the positive coefficient α_D, also of order $K^2\tau$. There are two reasons for the apparent discrepancy. First, the vertical advection of magnetic field occurs at the corners, where diffusion is inoperative. Consequently, though use of δ_0 in (3.4) is appropriate for the $\bar{b}_y$ field, the mechanism that it characterizes is not as potent for the $\bar{b}_x$ field which is not displaced so far. The importance of the diffusive effects is, therefore, overestimated by (3.6). Indeed, our detailed analysis of the later sections ignored vertical convection of the horizontal magnetic field in the boundary layers entirely. Secondly, as the numerical results of the following section show, the role of vertical advection in the corner regions (at least for small μ) is to lengthen the horizontal scale. It means that

† The t-dependence can also be ignored because of the relatively slow growth rate that ensues.

the flux sheet width ξ_0 (see (3.3*b*)) is an increasing function of β with the immediate consequence that $(\mathrm{d}\alpha/\mathrm{d}\beta)\,(0)$ is negative, as in (7.13*a*) above.

An interesting comparison can be made with the small-R calculations of the 'turbulent' diffusivity by Bullard & Gubbins (1977). In the appendix of that paper, they consider a double expansion in which the vertical velocity $K\psi$, like the vertical length scale l, is assumed to be large:

$$l = O(K), \quad K \gg 1, \quad R \ll 1. \tag{7.14a}$$

In that limit, the α-effect and 'turbulent' diffusivity are of comparable magnitude. Furthermore, the molecular and 'turbulent' diffusivities are comparable when

$$KR = O(1). \tag{7.14b}$$

With R small, the mean horizontal magnetic field is only perturbed weakly by the motion, but the dynamo mechanism remains essentially the same. In their model, 'turbulent' diffusion can be traced to the vertical advection of horizontal magnetic field exactly as in our heuristic calculation of α_{D} in (3.6). Their diffusivity, like α_{D}, is positive. Our results appear to indicate that, for fixed K, that the potency of the Bullard–Gubbins mechanism diminishes with increasing R. As explained in the previous paragraph, the corners play a key role when R is large. The long time τ spent near them provides an important additional parameter inapplicable to the Bullard & Gubbins (1977) analysis but upon which our analysis pivots.

Further insight into the question of positive and negative turbulent diffusivities is given by Parker (1979, Chap. 18) in his description of turbulence in perfectly conducting fluids. There he begins with the Cauchy solution (1.2) and assumes that the displacements of fluid particles from their initial positions, namely

$$\boldsymbol{\xi} = \boldsymbol{X} - \boldsymbol{x}, \tag{7.15a}$$

is small. It follows from (1.2) that

$$b_i(\boldsymbol{x}+\boldsymbol{\xi}, t) = b_j(\boldsymbol{x}, 0)\left(\delta_{ij} + \frac{\partial \xi_i}{\partial x_j}\right) \tag{7.15b}$$

and so the value of $\boldsymbol{b}(\boldsymbol{x}, t)$ can thus be obtained by an expansion procedure. Moffatt (1978, Chap. 7.10), like Parker (1979), adopts a similar approach and uses the result to calculate the mean EMF $\overline{\boldsymbol{u} \times \boldsymbol{b}}$. The point is that they both find two contributions to the turbulent diffusivity and Parker (1979, Chap. 18.4.2) illustrates them by a particular example. In it he shows that one contribution ($\langle \xi_z^2 \rangle$ in his (18.65)) comes from the displacement of magnetic field without distortion. It is essentially the diffusive mechanism which we described by (3.4) and which led to our positive diffusivity in (3.6). The other contribution ($-\langle \xi_z^2 \partial \xi_x / \partial x \rangle$ in his (18.65)) depends like the α-effect on the additional twist of the magnetic field. It is linked to our (7.13*a*). Parker (1979) points out through his example that this latter effect may be negative, as we have found for our problem.

7.2. *The case* $\mu = O(1)$

No approximations can be made to the boundary-layer equations when

$$\mu = O(1), \quad K^{-2} = O(\tau) \tag{7.16}$$

(or smaller). Since the formal development of §§4–6 hides many of the physical ideas leading to these complicated equations, a comparison problem is developed here. Its

purpose is to isolate the key issues that our theory must face. Quite simply the heat conduction equation

$$\theta_{,t}+(\boldsymbol{u}_{\mathrm{H}}\cdot\nabla)\theta = R^{-1}\nabla^2\theta. \tag{7.17}$$

is considered for some passive scalar θ. It generalizes (7.10) by restoring the z- and t-dependences and, in the notation of §4, it is simply

$$(\boldsymbol{u}_{\mathrm{H}}\cdot\nabla+\lambda)\tilde{\theta} = R^{-1}\nabla_{\mathrm{H}}^2\tilde{\theta}. \tag{7.18}$$

The assumption (7.16) implies that $K\beta$ is small;

$$K\beta = O(\tau^{-1}). \tag{7.19}$$

It means that the vertical lengthscale $R^{-\frac{1}{4}}\beta^{-1}$ is large compared to the horizontal lengthscale $R^{-\frac{1}{4}}$. With ν of order unity, (6.5*b*) implies that

$$\lambda = O(\tau^{-1}). \tag{7.20}$$

In turn, (7.20) leads to the boundary-layer approximation of §5, namely the neglect of the term $\lambda\tilde{\theta}$, in (7.18). It means that the contributions from vertical diffusion $\beta^2\tilde{\theta}$, vertical convection $\mathrm{i}(R^{\frac{1}{4}}w)\beta\tilde{\theta}$, and time dependence $p\tilde{\theta}$ are all negligible exactly as before in the Childress (1979) limit. Differences arise in the corner regions, where, because fluid particles take the long time τ to pass through, the term $\lambda\tilde{\theta}$ in (7.18) plays a significant role. The corner approximation of §6 is to neglect horizontal diffusion. The reduced form of (7.18),

$$(\boldsymbol{u}_{\mathrm{H}}\cdot\nabla)\tilde{\theta} = -\lambda\tilde{\theta}, \tag{7.21}$$

is readily solved giving, in the notation of §6, the result

$$\tilde{\theta}^{(0)} = \mathrm{e}^{-\lambda\tau}\tilde{\theta}^{(1)}, \tag{7.22}$$

where, of course, $\lambda\tau$ is of order unity.

The coefficient $\mathrm{e}^{-\lambda\tau}$ has three factors, $\mathrm{e}^{-p\tau}$, $\mathrm{e}^{-\beta^2\tau}$ and $\mathrm{e}^{\mathrm{i}\beta\tau(R^{\frac{1}{4}}w)}$. The first reflects the fact that (4.1*a*) assumes an amplification of $\mathrm{e}^{p\tau}$ in time τ, whereas there is no growth of θ, when $\theta_{,t}=0$! The second gives the decay due to vertical diffusion. It is, however, negligible within the framework of the approximation (7.19), i.e. $\beta^2\tau = O(K^{-2}\tau^{-1})$. The third and final contribution is interesting. It arises because fluid particles are displaced a significant vertical distance of order $R^{-\frac{1}{4}}K\tau$ (remember that $\tau \gg 1$) which is comparable with the vertical lengthscale $R^{-\frac{1}{4}}\beta^{-1}$. This process forms the basis of the 'stretch' dynamo mechanism described heuristically in §3. It leads to the possibility of bringing like-signed θ into close contact from either side of the vortex boundary $\psi = 0$ (see also figure 3). Indeed, figure 4(*b*) shows a sharp increase in the value of α_{S}, the α-'stretch' effect, when μ is roughly 0.2. It is reflected in the numerical results by a slow spatial decay of the eigenfunctions, particularly when μ lies between roughly 0.05 and 0.15. There, $0.05 \leqslant \mu \leqslant 0.17$, good convergence was obtained with $N = 36$, $\xi_1 = 1$, $\xi_N = 36.0$. For μ greater than 0.2 the decay distance shortens monotonically. The results illustrated in figure 4 have $\xi_1 = 0.5$ for $0.18 \leqslant \mu \leqslant 1.0$ and $\xi_1 = 0.25$ for $1.05 \leqslant \mu \leqslant 3.0$, while the corresponding value of ξ_N was systematically reduced. The spatial structure of the eigenfunctions themselves is not particularly illuminating. Just as in the case of small μ, for which Anufriyev & Fishman (1982) provide an illustration giving contours of constant A, the eigenfunctions exhibit the features of a spatially damped thermal wave (see (7.10), also the Appendix) induced by periodic forcing at the boundary $\xi = 0$.

7.3. *The case* $\mu \gg 1$

Some qualifications must be added to the remarks of the previous subsection when

$$\mu \gg 1. \tag{7.23a}$$

Obviously, if p increases, then the drop $e^{-p\tau}$ at the corners becomes more pronounced. Furthermore, if $\beta^2\tau$ remains small,

$$K^{-2}\mu^2 \ll \tau, \tag{7.23b}$$

vertical diffusion continues to be insignificant everywhere. On the other hand, the vertical advection at the corners has the dramatic effect of tilting the isotherms severely. As a result a fine structure of almost vertical bands of opposite-signed θ are produced on the horizontal lengthscale $R^{-\frac{1}{2}}\mu^{-1}$, which is much shorter than the boundary-layer width of order $R^{-\frac{1}{4}}$. This leads to considerable transverse diffusion in the outgoing boundary layer. Indeed, this is exactly what happens to $\tilde{A}_{,\xi}$ in (6.5), with the result that the 'stretch' contribution α_S to the α-effect is found to evaporate (see figure 4(*b*) and (7.26)). On the other hand, because of the symmetry of the vertical magnetic field produced in the corners, a small remnant flux $\pi K\overline{B}$, remains which is convected out along the boundary layer without any significant decay (see (7.3) and (7.30)). As μ increases, the α-effect, which now relies on the twist mechanism, decreases in strength. Nevertheless, within the framework of the neglect of vertical diffusion (the term $-(K\tau)^{-2}\mu^2$ in (7.4)), the dynamo operates with ever-increasing growth rate (i.e. $dp/d\mu > 0$, see (7.34*b*)).

An analytic solution of the governing equations is possible when μ is large because the integrals (5.13) and (6.7) can be evaluated asymptotically using the method of steepest descents. To begin with, the integral in (5.13*a*) is small, leaving

$$\tilde{A}_r(\sigma, \xi) = -\operatorname{erfc}\left[\frac{\xi}{(4\sigma)^{\frac{1}{2}}}\right] \quad (\mu^{-1} \ll \sigma < 2), \tag{7.24}$$

correct to leading order. The lower-order imaginary contribution to $\tilde{A}$ is determined by first noting that (6.5), (6.8) and (7.24) imply

$$\tilde{A}_1(0, \xi) \sim \tfrac{1}{2}\nu_0\mu^{-1}\, e^{-\xi^2/8} \sin(\mu\xi), \tag{7.25a}$$

where

$$\nu_0 = \left(\frac{2}{\pi}\right)^{\frac{1}{2}} e^{-\mu\nu}. \tag{7.25b}$$

The integral (5.13*a*) then gives

$$\tilde{A}_1(\sigma, \xi) \sim \tfrac{1}{2}(\pi\sigma)^{-\frac{1}{2}}\nu_0\mu^{-2}\, e^{-\xi^2/4\sigma} \quad (\mu^{-1} \ll \sigma < 2). \tag{7.26}$$

As explained in the previous paragraph, the fine structure produced at the corner on the flux scale $\xi = O(\mu^{-1})$ is rapidly diffused in the outgoing boundary layer leaving a very weak tongue of magnetic flux (7.26). It follows from (6.13*b*) that the small stretch contribution to the α-effect is

$$\nu_S = -\tfrac{1}{2}\mu^{-2}\nu_0. \tag{7.27}$$

The asymptotic evaluation of $\tilde{F}$ begins with (6.7). The leading-order term is

$$\begin{aligned}\tilde{F}^{(0)} &\sim e^{-\mu\nu - i\mu\xi}\int_\xi^\infty \xi' \tilde{A}^{(1)}_{r,\xi'}\, d\xi', \\ &= 2\nu_0\, e^{-i\mu\xi - \xi^2/8},\end{aligned} \tag{7.28}$$

by (7.24), (7.25b). With (6.12) it gives

$$\tilde{F}_1^{(i)}(0) = 2\nu_0, \tag{7.29}$$

which with (6.13a, c), (7.27) yields the central result

$$\nu \sim \nu_T \sim \nu_0, \quad \frac{\nu_S}{\nu_0} = O(\mu^{-2}). \tag{7.30a, b}$$

The value of $\tilde{F}$ in the boundary layer derived from (7.28), (6.8) and (5.13b) is

$$\tilde{F}(\sigma,\xi) \sim 2\nu_0\left\{\mathrm{i}\,\mathrm{erfc}\left[\frac{\xi}{(4\sigma)^{\frac{1}{2}}}\right] + (\pi\sigma)^{-\frac{1}{2}}\mu^{-1}\,\mathrm{e}^{-\xi^2/4\sigma}\right\} \quad (\mu^{-1} \ll \sigma < 2). \tag{7.31}$$

From (5.9), (5.11d) the corresponding value of $\tilde{B}$ is given by

$$\begin{aligned}\tilde{B}(\sigma,\xi) &= \tfrac{1}{2}(\tilde{F}_{,\xi} + \xi\tilde{A}_{,\xi}) \\ &\sim (\pi\sigma)^{-\frac{1}{2}}(-\mathrm{i}\nu_0 + \tfrac{1}{2}\xi)\,\mathrm{e}^{-\xi^2/4\sigma} \quad (\mu^{-1} \ll \sigma < 2).\end{aligned} \tag{7.32}$$

The twist contribution to the α-effect is linked with the production of vertical magnetic field (see (3.7) and (7.3) above). The corresponding value of α_T defined by (5.10b) is given in scaled form by (7.30a). It is, however, (7.32) that clarifies its origin. For even though the real (odd) part of $\tilde{B}$ dominates ($\nu_0 \ll 1$, see (7.34a)), it is the smaller imaginary (even) part which yields the result (7.30a).

Together (7.25b) and (7.30a) provide the solution to the eigenvalue problem, namely the function $\nu(\mu)$, which is the solution of

$$\nu = \left(\frac{2}{\pi}\right)^{\frac{1}{2}} e^{-\mu\nu}. \tag{7.33}$$

The plot of ν versus μ is given by the broken curve of figure 4(a). By $\mu = 4.0$ it shows good convergence to the solid curve obtained by numerical integration of the complete boundary-layer equations. It should be emphasized, however, that fine spatial resolution is required to resolve the factors $\mathrm{e}^{\mathrm{i}\mu\xi}$, which appear in the integrals. Indeed, the numerical solution at $\mu = 4.0$ required $N = 62$, $\xi_1 = 0.125$, $\xi_N = 7.75$ in order to obtain satisfactory results. The large-μ behaviour, which is well established at $\mu = 4.0$, is clearly evident in figure 4(a, b) when μ is as small as unity. Indeed, even by $\mu = 0.5$ the α-'stretch' effect has largely disappeared. Finally, note that, for large μ, (7.33) can be solved giving an awkward asymptotic expansion whose leading term is

$$\nu \sim \mu^{-1}\ln\mu, \tag{7.34a}$$

which with (7.4) gives

$$p \sim \tau^{-1}\ln\mu \quad (1 \ll \mu \ll \tau). \tag{7.34b}$$

7.4. *The maximum growth rate*

The slow increase of growth rate p with β exhibited by (7.34b) cannot continue indefinitely. Indeed (4.8c), (5.1a), (7.4) and (7.33) give

$$p = \left(\frac{2}{\pi}\right)^{\frac{1}{2}}\beta K\,\mathrm{e}^{-(p+\beta^2)\tau} - \beta^2, \tag{7.35}$$

and differentiation yields the expression

$$(p_{\max} + \beta_{\max}^2)^{-1} = \tfrac{1}{2}\beta_{\max}^{-2} - \tau, \tag{7.36a}$$

for the maximum growth rate $p_{\max}$, which occurs when $\mathrm{d}p/\mathrm{d}\beta = 0$ at $\beta = \beta_{\max}$ (say). Correct to leading order (7.35) and (7.36*a*) are satisfied when

$$\beta_{\max} \sim (2\tau)^{-\frac{1}{2}}, \quad p \sim (2\tau)^{-1} \ln \tau. \tag{7.36b, c}$$

Evidently $\beta_{\max}$ is small as required by our asymptotic theory. On the other hand, as (7.4) makes clear, the result (7.36) depends on the low-order term β^2 in (7.35). At that level, other terms may be present that our zeroth-order analysis fails to predict. It should be emphasized, however, that the value of $p_{\max}$ is not particularly sensitive to the terms β^2. To leading order the result is the same if β^2 is replaced by $M\beta^2$ for any positive constant M. It is, therefore, likely that (7.36*b*) provides a reasonable estimate of the maximum growth rate. For the $\epsilon = 0$ case, (2.8*b*) and (7.36) yields the result

$$p_{\max} \sim \frac{\ln(\ln R)}{\ln R}, \tag{7.37a}$$

which occurs when the vertical wavenumber is

$$R^{\frac{1}{2}}\beta_{\max} \sim \left(\frac{R}{\ln R}\right)^{\frac{1}{2}} \quad \text{as } R \uparrow \infty. \tag{7.37b}$$

7.5. *The Roberts' dynamo*

It is fortunate that Roberts (1972) has provided such a thorough and comprehensive set of numerical results for his first motion, which coincides with our $\epsilon = 0$, Beltrami case (2.10). Since his results are obtained at finite values of R, whereas ours are valid as $R \uparrow \infty$, a comparison of the two provides a useful independent check of both analyses. Though our boundary-layer approximations appear to be based on expansions involving $\tau^{-1} (\equiv 2/\ln R)$ (see (2.8*b*), (5.1*b*)), which is itself linked with R, closer inspection reveals that $K\beta$ is, instead, the natural expansion parameter (see (5.1*c*)). We stress the existence of two independent parameters, R^{-1} and $K\beta$, because it proves useful in the comparisons that follow.

Since Roberts (1972) used different coordinates (see the end of §2) a preliminary change of variables is necessary. With $K = \sqrt{2}$, $\lambda^{(\mathrm{R})}$, $\alpha^{(\mathrm{R})}$ and j are related to our R, α and β (the superscript R is used to avoid confusion with our variables) by

$$\lambda^{(\mathrm{R})} = \frac{2}{R}, \quad \alpha^{(\mathrm{R})} = \left(\frac{2}{R}\right)^{\frac{1}{2}}\alpha, \quad j = (\tfrac{1}{2}R)^{\frac{1}{2}}\beta, \tag{7.38a}$$

or alternatively from (2.8*b*) and (5.1*a*),

$$-\alpha^{(\mathrm{R})} = 2R^{-\frac{1}{2}}\nu, \quad j = \left(\frac{R^{\frac{1}{2}}}{\ln R}\right)\mu. \tag{7.38b}$$

The corresponding formula (7.4) for the growth rate is

$$p = \left(\frac{2\mu}{\ln R}\right)\left(\nu - \frac{\mu}{\ln R}\right). \tag{7.38c}$$

For the case $j \ll 1$ (i.e. small β), table 3 of Roberts (1972) lists $|\alpha^{(\mathrm{R})}|$ for various values of $\lambda^{(\mathrm{R})}$. This is the Childress (1979) small-μ limit of §7.1. In table 1 the values for $\lambda^{(\mathrm{R})}$ less than unity are translated into our primitive R, ν variables. It is encouraging to find that the value of ν for $R = 16$, 32 and 64 differs from our value (7.6) by less than 2%. On the other hand, the value for $R = 128$ is badly out of line and must be interpreted cautiously. Indeed, Roberts (1972) does not claim three-

R	4	8	16	32	64	128
$\lambda^{(R)}$	$\frac{1}{2}$	$\frac{1}{4}$	$\frac{1}{8}$	$\frac{1}{16}$	$\frac{1}{32}$	$\frac{1}{64}$
$\lvert\alpha^{(R)}\rvert$	0.620	0.394	0.266	0.187	0.131	0.085
ν	0.620	0.557	0.532	0.529	0.524	0.48

TABLE 1. The α-effect ν predicted in the limit $\mu \to 0$ by Roberts' (1972) numerical results for $\alpha^{(R)}$

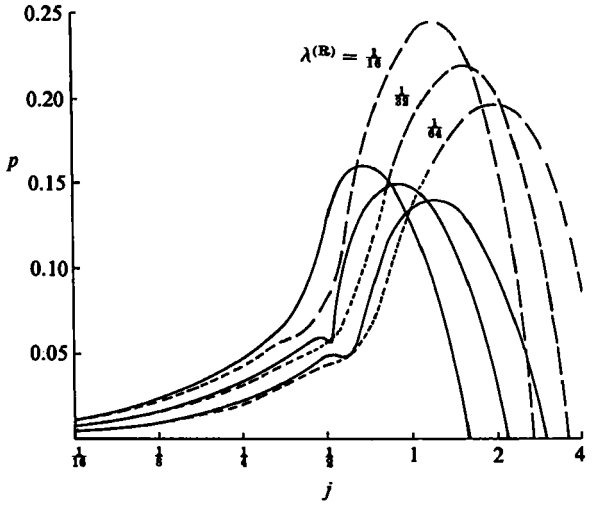

FIGURE 5. A comparison of Roberts (1972) numerical results with our asymptotic results. The solid curves, which are reproduced directly from Roberts (1972, figure 7), give the growth rate p plotted versus j for various values of $\lambda^{(R)}$ (see (7.34a, b)). Our asymptotic results are plotted broken. The short (long)-broken curves correspond to the regimes in which $\mu/(\nu \ln R)$ is less (greater) than $\frac{1}{8}$ (see (7.38c)) and where $\nu(\mu)$ is given by figure 4(a).

significant-figure accuracy for that case which would appear to be at the limit of his numerical capability.

The complete picture of Roberts' (1972) numerical results are summarized in his figure 7, which plots growth rate p versus wavenumber j for the nine distinct cases $\lambda^{(R)} = 2^{-N}$ ($N = -2, -1, 0, 1, \ldots, 6$). For small λ, specifically $N \geqslant 3$, the curves illustrated in his figure exhibit similarity form: the last three ($N = 4, 5, 6$) are reproduced here as the solid curves in figure 5. This observation is consistent with the evidence of table 1 that asymptotic behaviour is beginning to emerge with R as low as 16. To test this possibility further our numerical representation of the function $\nu(\mu)$ illustrated in figure 4(a) is used to plot p versus j as the broken curves on figure 5 for the same three cases, namely $R = 32, 64, 128$.

Since our expansion scheme has assumed that $\mu/\ln R$ is small, our results plotted in figure 5 become less reliable as j increases. In an attempt to quantify the reliability, the curves are short-broken when the ratio of the diffusivity term to the α-effect term $\mu/(\nu \ln R)$ is less than $\frac{1}{8}$ and long-broken otherwise. The short-broken curves agree well with Roberts' (1972) results but significant quantitative differences are apparent for the long-broken curves on which $\mu/(\nu \ln R)$ exceeds $\frac{1}{8}$. As already explained, we do not

expect our theory to be valid when $\mu/\ln R$ is of order unity and any similarity of the results is purely fortuitous.

An intriguing feature of Roberts' (1972) results, which clearly caused him some concern, is his kink on the solid curves which occurs when j is close to $\frac{1}{2}$ (see figure 5). The same feature is evident on our short-broken curves, though not so pronounced. Its origin, however, is clear from figure 4(*a*). Apparently, as β increases, the strength of the α-effect drops slightly and is then followed by a sudden rise. In turn, this parameter-sensitive behaviour is linked with the dramatic increase of α_S illustrated by the plot of ν_S in figure 4(*b*). It means that kink isolated by Roberts (1972) occurs when the α-'stretch' effect is working at its best. Nevertheless, the intensity of the process is largely offset by the α-'twist' effect which adjusts its value so that changes in the total α-effect are less pronounced. The identification of this kink and the explanation of the underlying dynamo mechanisms constitute the main successes of the present asymptotic analysis.

8. Concluding remark

The boundary-layer development of this paper has identified fast dynamo mechanisms that can operate in certain simple spatially periodic flows. The fact that a weak singularity at the X-type stagnation points is necessary (the case $\epsilon \neq 0$) for the dynamo to be fast is in itself significant. The point is simply that magnetic flux in any large-magnetic-Reynolds-number dynamo caused by steady flow is likely to be confined in sheets or ropes which lie on streamlines passing through stagnation points. Since the flow velocity vanishes at the stagnation points, the long time τ, of order $\ln R$, taken for fluid particles to pass by is likely to limit the speed of the dynamo for physically realistic flows. It must, however, be stressed that our analysis is only concerned with integrable flows, the picture for the non-integrable flows investigated by Galloway & Frisch (1986) is less clear. Recent investigations (see Childress 1979; Childress & Soward 1984; Ghil & Childress 1986; Soward & Childress 1986) suggest that an α-effect of order unity may be possible. If the mean magnetic field produced by it can exist on a lengthscale comparable with the motion, then growth rates of order unity can be expected. For the moment these ideas are purely speculative as the quantitative evidence is slim.

I am grateful to S. Childress, H. K. Moffatt and an anonymous referee for their helpful remarks and constructive criticisms. I have also benefitted from discussions with C. A. Jones, M. R. E. Proctor, G. O. Roberts and P. H. Roberts.

Appendix

Until now an analytic solution of Childress' heat-conduction problem has proved elusive (see Childress 1979; Roberts 1979). That such a solution exists is suggested strongly by Anufriyef & Fishman's (1982) numerical discovery of the number (A 23) below. The problem consists of finding the periodic solution

$$\theta(\sigma+8,\xi) = \theta(\sigma,\xi) \tag{A 1}$$

of the heat conduction equation

$$\theta_{,\sigma} = \theta_{,\xi\xi} \tag{A 2}$$

on $\xi > 0$ which satisfies the boundary conditions

$$\theta(\sigma,0) = \begin{cases} -1 & (0<\sigma<2), \\ 1 & (4<\sigma<6), \end{cases} \tag{A 3a}$$

$$\theta_{,\xi}(\sigma,0) = 0 \qquad (2<\sigma<4, \quad 6<\sigma<8), \tag{A 3b}$$

$$\theta(\sigma,\xi) \to 0 \qquad \text{as } \xi \uparrow \infty. \tag{A 3c}$$

Its analytic solution outlined here is obtained using the Wiener–Hopf technique, as Childress (1979) suggested.

The analysis begins with the introduction of the complex function

$$\bar{A}(\sigma,\xi) = \theta(\sigma,\xi) + \mathrm{i}\theta(\sigma+2,\xi). \tag{A 4}$$

With the boundary conditions (A 3), the periodicity condition (A 1) can be strengthened to $\theta(\sigma+4,\xi) = -\theta(\sigma,\xi)$ which in turn implies that

$$\bar{A}(\sigma-2,\xi) = \mathrm{i}\bar{A}(\sigma,\xi), \tag{A 5}$$

consistent with (6.5) and (6.8), where $\lambda = 0$. It is easy to show that, in terms of $\theta(0,\xi)$ and $\theta(2,\xi)$, the Green function solution of (A 2) and (A 3) on the interval $0 < \sigma < 4$ is simply (5.13*a*).

When (5.13*a*) and (A 5) are evaluated at $\sigma = 2$, they yield an integral equation for $\bar{A}(2,\xi)$. Differentiation of that equation with respect to ξ gives

$$\phi(\xi) = \frac{1+\Gamma}{(2\pi)^{\frac{1}{2}}} \mathrm{e}^{-\xi^2/8} + \frac{\mathrm{i}}{(8\pi)^{\frac{1}{2}}} \int_0^\infty [\phi(\xi') \, \mathrm{e}^{-(\xi-\xi')^2/8} - \phi^*(\xi') \, \mathrm{e}^{-(\xi+\xi')^2/8}] \, \mathrm{d}\xi', \quad \text{on } 0<\xi<\infty, \tag{A 6}$$

where

$$\phi(\xi) = \bar{A}_{,\xi}(2,\xi) \tag{A 7}$$

and the constant Γ is defined by

$$1 + \mathrm{i}\Gamma = -\bar{A}(2,0) = \int_0^\infty \phi \, \mathrm{d}\xi. \tag{A 8}$$

The principle quantity of interest is the total heat $\int_0^\infty \theta \, \mathrm{d}\xi$, which remains constant on the insulating interval $2 < \sigma < 4$. Its value, which defines the number (3.13*b*), is

$$-2\nu_{\mathrm{C}} = -\mathrm{Im}\left[\int_0^\infty \xi\phi \, \mathrm{d}\xi\right]. \tag{A 9}$$

while ν_{C}, so defined, is the leading-order coefficient in the expansion (7.6).

The boundary conditions

$$Re\,[\bar{A}_{,\xi\xi}(\sigma,0)] = \mathrm{Im}\,[A_{,\xi}(\sigma,0)] = 0 \quad \text{on } 0<\sigma<2, \tag{A 10}$$

mean that ϕ can be extended naturally to negative ξ upon defining

$$\phi(-\xi) = \phi^*(\xi). \tag{A 11}$$

By this device, it is readily established that (A 6) holds everywhere, $-\infty < \xi < \infty$, and not simply on the semi-infinite positive interval. To simplify the analysis we make the change of variables

$$\xi = \sqrt{8}x. \tag{A 12}$$

The crucial step (A 11) now enables us to take the Fourier transform of (A 6), which yields

$$\hat{\phi}_+ + \hat{\phi}_- = \left[\frac{1+\Gamma}{\sqrt{2}} + \mathrm{i}(\hat{\phi}_+ - \hat{\phi}_-)\right] \mathrm{e}^{-k^2/4}, \tag{A 13}$$

where

$$\hat{\phi}_+(k) = \int_0^\infty \phi\, \mathrm{e}^{\mathrm{i}kx}\, \mathrm{d}x, \tag{A 14a}$$

$$\hat{\phi}_-(k) = \int_{-\infty}^0 \phi\, \mathrm{e}^{\mathrm{i}kx}\, \mathrm{d}x. \tag{A 14b}$$

In view of (A 11) $\hat{\phi}_\pm$ has the property

$$\hat{\phi}_-(k) = \hat{\phi}_+^*(k), \tag{A 15}$$

for real k, which suggests that (A 13) should be written in the alternative form

$$\mathrm{e}^{-\mathrm{i}\pi/4}\left[\hat{\phi}_+ - \frac{\mathrm{i}(1+\Gamma)}{\sqrt{8}}\right] \sinh\left(\tfrac{1}{8}k^2 - \mathrm{i}\tfrac{1}{4}\pi\right) = \mathrm{e}^{\mathrm{i}\pi/4}\left[\hat{\phi}_- + \frac{\mathrm{i}(1+\Gamma)}{\sqrt{8}}\right] \sinh\left(\tfrac{1}{8}k^2 + \mathrm{i}\tfrac{1}{4}\pi\right). \tag{A 16}$$

The form (A 16) leads to a relatively straightforward Wiener–Hopf problem which can be solved by standard methods. The key step is to write

$$\sinh z = z \prod_{n=1}^{\infty} \left[1 + \left(\frac{z}{n\pi}\right)^2\right] \tag{A 17}$$

(see, for example, Abramowitz & Stegun 1965, p. 85) and to factorize (A 16) into the form

$$B_+(k) = B_-(k)\,(= B, \text{ say}), \tag{A 18}$$

where $B_+(k)$ and $B_-(k)$ are analytic in the upper and lower halves of the complex k-plane. That means that B is analytic everywhere and consequently a constant independent of k. Its value is fixed by the condition that

$$\hat{\phi}_+(k) \to 0 \quad \text{as } \operatorname{Im} k \uparrow \infty, \tag{A 19}$$

or equivalently $\hat{\phi}_-(k) \to 0$ as $\operatorname{Im} k \downarrow -\infty$. The result is

$$\hat{\phi}_+(k) = \frac{1+\Gamma}{\sqrt{8}} \left\{\mathrm{i} - \mathrm{e}^{\mathrm{i}\pi/4} \frac{k + (-1+\mathrm{i})\,\pi^{\frac{1}{2}}}{k + (1+\mathrm{i})\,\pi^{\frac{1}{2}}} \prod_{n=1}^{\infty} D_n(k)\right\}, \tag{A 20a}$$

where

$$D_n(k) = \frac{\{k + (-1+\mathrm{i})\,[(4n+1)\,\pi]^{\frac{1}{2}}\}\,\{k + (1+\mathrm{i})\,[(4n-1)\,\pi]^{\frac{1}{2}}\}}{\{k + (1+\mathrm{i})\,[(4n+1)\,\pi]^{\frac{1}{2}}\}\,\{k + (-1+\mathrm{i})\,[(4n-1)\,\pi]^{\frac{1}{2}}\}}. \tag{A 20b}$$

Here we have used the property

$$\lim_{\operatorname{Im} k \uparrow \infty} \left\{\sum_{n=1}^{\infty} \ln D_n(k)\right\} = \mathrm{i}\tfrac{1}{4}\pi, \tag{A 21}$$

which fixes B by guaranteeing (A 19).

The unknown constant Γ is now determined by application of the condition (A 8). It gives

$$1 + \mathrm{i}\Gamma = \sqrt{8}\hat{\phi}_+(0). \tag{A 22a}$$

With (A 20) it reduces to

$$1 + \mathrm{i}\Gamma = (1+\Gamma)\,\mathrm{i}(1 - \mathrm{e}^{\mathrm{i}\pi/4}), \tag{A 22b}$$

which is satisfied when

$$\Gamma = \sqrt{2} - 1. \tag{A 23}$$

This is the result reported by Anufriyev & Fishman (1982, end of §4). They confirm (A 23) by their numerical method correct to five significant figures. The formal mathematical solution of the integral equation (A 6) is now complete. It is

$$\phi(\xi) = \frac{1}{2\pi}\int_{-\infty}^{\infty} [\hat{\phi}_+(k)+\hat{\phi}_-(k)]\,\mathrm{e}^{-\mathrm{i}k\xi/\sqrt{8}}\,\mathrm{d}k, \tag{A 24}$$

in which $\hat{\phi}_+$ and $\hat{\phi}_-$ are defined by (A 15), (A 20) and (A 23). Clearly this integral can be expressed as an infinite sum by evaluating the residues of $\hat{\phi}_+$ and $\hat{\phi}_-$ at the simple poles. That is easily done but the coefficients in the resulting infinite series are given by infinite products, whose numerical values are difficult to obtain. The procedure leads to the harmonic expansion proposed by Roberts (1979, equations (B 1), (B 2)) and employed by Anufriyev & Fishman (1982, equation (14)).

Finally the results can be used to calculate the total heat, $\int_0^\infty \theta(4,\xi)\,\mathrm{d}\xi$, defined by (A 9). In terms of the Fourier integral (A 14) the value of ν_C is

$$\nu_C = -4\,\mathrm{Re}\left[\frac{\mathrm{d}\hat{\phi}_+}{\mathrm{d}k}\right]_{k=0}. \tag{A 25}$$

The evaluation of ν_C is simplified by expressing (A 25) in the alternative form

$$\nu_C = -4\,\mathrm{Re}\left\{(\hat{\phi}_+(0)-\tfrac{1}{2}\mathrm{i})\left[\frac{\mathrm{d}\{\ln(\hat{\phi}_+(k)-\tfrac{1}{2}\mathrm{i})\}}{\mathrm{d}k}\right]_{k=0}\right\}. \tag{A 26}$$

Direct substitution of (A 20*a*) yields the result

$$\nu_C = \left(\frac{2}{\pi}\right)^{\frac{1}{2}} \sum_{n=1}^{\infty} \frac{(-1)^n}{(2n+1)^{\frac{1}{2}}} \tag{A 27a}$$

$$= 0.532\,740\,705\,0\ldots. \tag{A 27b}$$

REFERENCES

Abramowitz, M. & Stegun, I. A. (eds) 1965 *Handbook of Mathematical Functions*. Dover.

Anufriyev, A. P. & Fishman, V. M. 1982 Magnetic field structure in the two-dimensional motion of a conducting fluid. *Geomag. Aeron.* **22**, 245–248.

Arnol'd, V. I. & Korkina, E. I. 1983 The growth of a magnetic field in a steady incompressible flow. *Vest. Mosk. Un. Ta. Ser. 1, Math. Mec.* **3**, 43–46 (in Russian).

Braginsky, S. I. 1964 Self-excitation of a magnetic field during the motion of a highly conducting fluid. *Z. Eksp. teor. Fiz.* **47**, 1084–1098. (Transl. *Sov. Phys., J. Exp. Theor. Phys.* **20**, (1965) 726–735).

Bullard, E. C. & Gubbins, D. 1977 Generation of magnetic fields by fluid motions of global scale. *Geophys. Astrophys. Fluid Dyn.* **8**, 43–56.

Busse, F. H. 1978 Introduction to the theory of geomagnetism. In *Rotating Fluids in Geophysics* (ed. P. H. Roberts & A. M. Soward), pp. 361–388. Academic.

Childress, S. 1967 Construction of steady-state hydromagnetic dynamos. 1. Spatially periodic fields. *Courant Institute of Mathematical Sciences Rep.* MF-53, pp. 1–36.

Childress, S. 1970 New solutions of the kinematic dynamo problem. *J. Math. Phys.* **11**, 3063–3076.

Childress, S. 1979 Alpha-effect in flux ropes and sheets. *Phys. Earth Planet. Int.* **20**, 172–180.

Childress, S. & Soward, A. M. 1984 On the rapid generation of magnetic fields. In *Chaos in Astrophysics*, Nato Advanced Research Workshop, Palm Coast, Florida, USA.

Dombre, T., Frisch, U., Greene, J. M., Hénon, M., Mehr, A. & Soward, A. M. 1986 Chaotic streamlines and Lagrangian turbulence: the ABC flows. *J. Fluid Mech.* **167**, 353–391.

Galloway, D. J. & Frisch, U. 1984 A numerical investigation of magnetic field generation in a flow with chaotic streamlines. *Geophys. Astrophys. Fluid Dyn.* **29**, 13–18.

GALLOWAY, D. & FRISCH, U. 1986 Dynamo action in a family of flows with chaotic streamlines. *Geophys. Astrophys. Fluid Dyn.* **36**, 53–83.

GHIL, M. & CHILDRESS, S. 1986 *Topics in Geophysical Fluid Dynamics: Atmospheric Dynamics, Dynamo Theory and Climate Dynamics*. Applied Mathematical Science Series. Springer.

KRAUSE, F. & RÄDLER, K.-H. 1980 *Mean-Field Magnetohydrodynamics and Dynamo Theory*. Akademic-Verlag and Pergamon.

MOFFATT, H. K. 1970 Turbulent dynamo action at low magnetic Reynolds number. *J. Fluid Mech.* **41**, 435–452.

MOFFATT, H. K. 1978 *Magnetic Field Generation in Electrically Conducting Fluids*. Cambridge University Press.

MOFFATT, H. K. & PROCTOR, M. R. E. 1985 Topological constraints associated with fast dynamo action. *J. Fluid Mech.* **154**, 493–507.

PARKER, E. N. 1979 *Cosmical Magnetic Fields*. Clarendon.

ROBERTS, G. O. 1972 Dynamo action of fluid motions with two-dimensional periodicity. *Phil. Trans. R. Soc. Lond.* A **271**, 411–454.

ROBERTS, G. O. 1979 Fast viscous Bénard convection. *Geophys. Astrophys. Fluid Dyn.* **12**, 235–272.

SOWARD, A. M. & CHILDRESS, S. 1986 Analytic theory of dynamos. *Adv. Space Res. Proc. COSPAR meeting, Toulouse* (to appear).

VAINSHTEIN, S. I. & ZEL'DOVICH, YA. B. 1972 Origin of magnetic fields in astrophysics. *Sov. Phys. Usp.* **15**, 159–172.

WEISS, N. O. 1966 The expulsion of magnetic flux by eddies. *Proc. R. Soc. Lond.* A **293**, 310–328.

ZEL'DOVICH, YA. B., RUZMAIKIN, A. A., MOLCHANOV, S. A. & SOKOLOV, D. D. 1984 Kinematic dynamo problem in a linear velocity field. *J. Fluid Mech.* **144**, 1–11.

ZEL'DOVICH, YA. B., RUZMAIKIN, A. A. & SOKOLOV, D. D. 1983 *Magnetic Fields in Astrophysics*. Gordon & Breach.